SONNE -Berichte

Conjoint Monitoring of the Ocean Bottom offshore Chile Humboldt Organic MattEr Remineralization

Cruise No. SO 288

15.01.2022 – 15.02.2022,
Guayaquil (Ecuador) – Valparaiso (Ecuador)
COMBO & HOMER

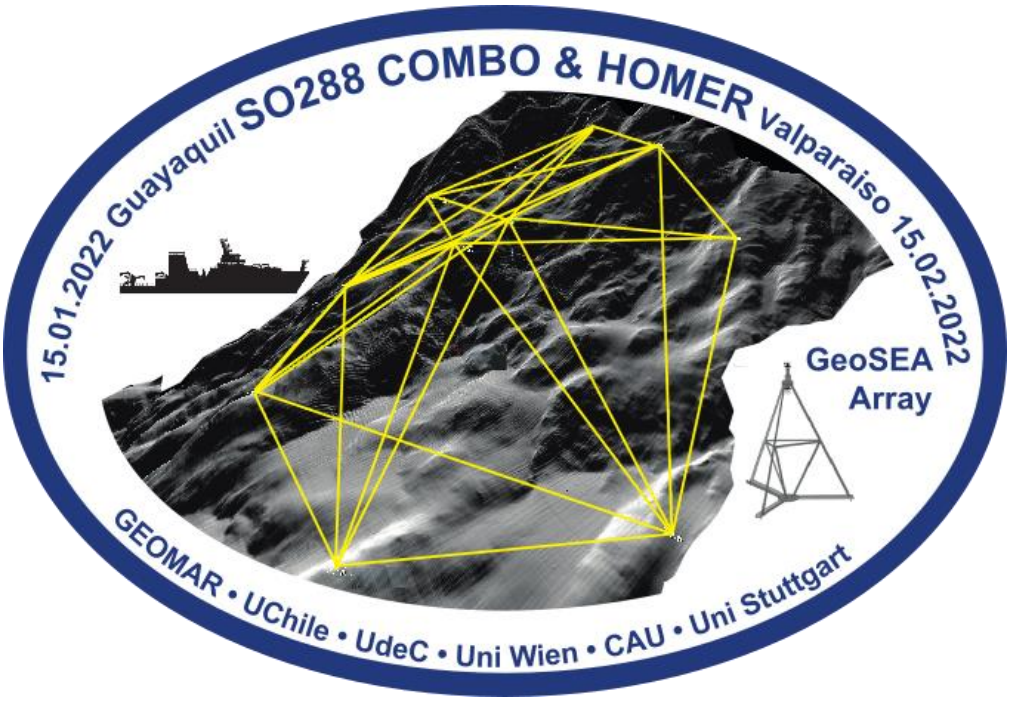

H.Kopp and all Cruise Participants

GEOMAR Helmholtz Centre for Ocean Research Kiel

2022

Table of Contents

1 Cruise Summary

1.1 Summary in English

Cruise SO288 served two scientific projects. The main objective of the COMBO project was the recovery of three seafloor geodetic networks of the GeoSEA array which were installed on the continental margin and outer rise offshore Iquique in northern Chile during RV SONNE cruise SO244. This work was flanked by additional seismic and bathymetric surveys to characterize the sub-seafloor structure. The South American subduction system around 21°S has last ruptured in an earthquake in 1877 and was identified as a seismic gap prior to the 2014 Iquique earthquake (Mw=8.1). The southern portion of the segment remains unbroken by a recent earthquake and is currently in the latest stage of the interseismic phase of the seismic cycle. The seafloor geodetic measurements of the GeoSEA array provide a way to monitor crustal deformation at high resolution comparable to the satellite-based GPS technique upon which terrestrial geodesy is largely based. The GeoSEA array consists of autonomous seafloor transponders installed on 4 m high tripods. The transponders within an array intercommunicate via acoustic signals for a period of up to three years. Recovery of the GeoSEA array using a remotely operated vehicle (ROV KIEL6000) required dedicated dives in the three network locations on the middle and lower continental slope (AREA1 and AREA3, respectively) and the outer rise of the Nazca plate (AREA2). All 23 GeoSEA transponders were successfully recovered and showed an 100% uptime during the monitoring period. The GeoSEA survey represents the first seafloor geodetic transect across a subduction zone, spanning from the oceanic outer rise to the lower and middle slope of the continental upper plate.

The second project, HOMER, focused on biogeochemical and microbiological processes that affect carbon cycling of the Humboldt Current System off Northern Chile down to the deep ocean. For this purpose, water samples were collected for the detailed chemical characterization of organic matter and the activity of microorganisms. The work was complemented by onboard incubations of microbial populations from deep waters with naturally occurring organic matter.

Cruise SO288 was the first expedition of RV SONNE back to the Pacific Ocean starting from a South American port during the COVID-19 pandemic. Despite strict safety and health requirements prior to boarding RV SONNE in Guayaquil, several members of the scientific and ship’s crew tested positive to COVID-19 two days after we left port. Containment measures were immediately put to action, flanked by a tight testing regime. Ten days after leaving Guayaquil, we were able to break the chains of infection and the scientific working program commenced.

1.2 Zusammenfassung

Die Fahrt SO288 ist in zwei wissenschaftliche Projekte eingebettet. Das Hauptziel des COMBO-Projekts war die Bergung von drei geodätischen Netzwerken des GeoSEA-Arrays, die während der Fahrt SO244 des FS SONNE am unteren und mittleren Kontinentalhang und auf der ozeanischen Platte vor Iquique in Nordchile installiert wurden. Diese Arbeiten wurden durch zusätzliche seismische und bathymetrische Untersuchungen flankiert, um die Struktur des Meeresbodens zu charakterisieren. Das südamerikanische Subduktionssystem um 21°S wurde zuletzt 1877 durch ein Erdbeben durchbrochen und wurde vor dem Iquique-Erdbeben 2014 (Mw=8,1) als seismische Lücke identifiziert. Der südliche Teil des Segments wurde noch nicht

von einem neueren Erdbeben erfasst und befindet sich derzeit in der letzten Phase der interseismischen Periode des seismischen Zyklus. Die geodätischen Messungen des GeoSEA-Arrays am Meeresboden ermöglichen die Überwachung der Krustendeformation mit einer hohen Auflösung, die mit der satellitengestützten GPS-Technik vergleichbar ist, auf der die terrestrische Geodäsie weitgehend beruht. Das GeoSEA-Array besteht aus autonomen Meeresbodentranspondern, die auf 4 m hohen Tripoden installiert sind. Die Transponder innerhalb eines Arrays kommunizieren über akustische Signale für einen Zeitraum von bis zu drei Jahren miteinander. Die Bergung des GeoSEA-Arrays mit einem ferngesteuerten Fahrzeug (ROV KIEL6000) erforderte spezielle Tauchgänge an den drei Standorten des Netzwerks am mittleren und unteren Kontinentalhang (AREA1 bzw. AREA3) und auf der ozeanischen Nazca-Platte (AREA2). Alle 23 GeoSEA-Transponder wurden erfolgreich geborgen und haben während des Überwachungszeitraums zu 100 % gesendet. Die GeoSEA-Vermessung stellt den ersten geodätischen Meeresbodentransekt über eine Subduktionszone dar, der sich von der ozeanischen Platte bis zum unteren und mittleren Hang der oberen Kontinentalplatte erstreckt.

Das zweite Projekt, HOMER, konzentrierte sich auf biogeochemische und mikrobiologische Prozesse, die den Kohlenstoffkreislauf des Humboldtstromsystems vor Nordchile bis in die Tiefsee beeinflussen. Zu diesem Zweck wurden Wasserproben zur detaillierten chemischen Charakterisierung organischer Stoffe und zur Untersuchung der Aktivität von Mikroorganismen entnommen. Ergänzt wurden die Arbeiten durch Inkubationen von Mikroorganismen-populationen aus der Tiefsee mit natürlich vorkommenden organischen Stoffen an Bord.

Die Fahrt SO288 war die erste Expedition des FS SONNE, die während der COVID-19-Pandemie von einem südamerikanischen Hafen aus zurück in den Pazifischen Ozean fuhr. Trotz strenger Sicherheits- und Gesundheitsvorschriften vor dem Einschiffen auf FS SONNE in Guayaquil wurden mehrere Mitglieder des wissenschaftlichen Teams und der Schiffsbesatzung zwei Tage nach dem Auslaufen aus dem Hafen positiv auf COVID-19 getestet. Es wurden sofort Eindämmungsmaßnahmen ergriffen, die von einem strengen Testregime flankiert wurden. Zehn Tage nach dem Auslaufen aus Guayaquil konnten wir die Infektionskette durchbrechen und das wissenschaftliche Arbeitsprogramm aufnehmen.

2 Participants

2.1 Principal Investigators

Name	Institution
Kopp, Heidrun, Prof. Dr.	GEOMAR
Lange, Dietrich, Dr.	GEOMAR
Abegg, Friedrich, Dr.	GEOMAR
Becker, Kevin, Dr.	GEOMAR
Pontiller, Benjamin, Dr.	GEOMAR

2.2 Scientific Party

Name	Discipline	Institution
Kopp, Heidrun, Prof. Dr.	Seafloor Geodesy / Chief Scientist	GEOMAR

Lange, Carl Dietrich, Dr.	Seafloor Geodesy / Co-Chief	GEOMAR
Abegg, Friedrich, Dr.	Head of ROV	GEOMAR
Becker, Kevin, Dr.	Leading scientist Biology	GEOMAR
Pontiller, Benjamin, Dr.	Biology	GEOMAR
Kuehn, Michel	Streamer	GEOMAR
Murray-Bergquist, Louisa	Bathymetry / OBS	GEOMAR
Flerus, Ruth, Dr.	Technician Biology	GEOMAR
Pieper, Martin	Technician ROV	GEOMAR
Striewski, Peter	Technician ROV	GEOMAR
Huusmann, Hannes	Technician ROV	GEOMAR
Cuno, Patrick	Technician ROV	GEOMAR
Suck, Inken, Dr.	Technician ROV	GEOMAR
Bodendorfer, Matthias	Technician ROV	GEOMAR
Matthiessen, Torge	Technician ROV	GEOMAR
Bartels, Thies	Airguns / OBS / Streamer	GEOMAR
Rohde, Lea	Airguns / OBS / Streamer	GEOMAR
Filbrandt, Christian	Seafloor Geodesy / Airguns	CAU
Thomas, Bruce	Seafloor Geodesy	Uni Stuttgart
Kontradowitz, Stefan	Seafloor Geodesy / OBS	GEOMAR
Moegeltoender, Jasmin	Seafloor Geodesy / Streamer	GEOMAR
Rosmann, Mara	Biology	CAU
Amano, Chie	Ultrasound / Temperature / CTD	Uni Wien
Maehnert, Barbara	Ultrasound / Temperature / CTD	Uni Wien
Carrillo, Vanessa	Seafloor Geodesy / Bathymetry	UChile
Hormazabal, Joaquin	Seafloor Geodesy / Bathymetry	UChile

2.3 Participating Institutions

GEOMAR	Helmholtz-Zentrum für Ozeanforschung Kiel
CAU	Christian-Albrechts-Universität zu Kiel
UChile	Universidad de Chile, Santiago
	Universität Stuttgart
	Universität Wien

3 Research Program

3.1 Description of the Work Area

The South American trench system offshore northern Chile marks the location of the convergent margin where the oceanic Nazca plate actively subducts underneath the continental upper plate of South America. This process causes recurrent large earthquakes (M>8) when the shallow plate interface ruptures. The Chilean subduction zone is almost exclusively located beneath the marine forearc and has been the site of a number of large earthquakes in the recent past, including the 2014 Iquique event with a magnitude of Mw=8.1 (e.g. Lay et al., 2014) which ruptured the plate boundary between 19.5°-21°S. Plate convergence between the Nazca and South America plates

occurs at a rate of 65 mm/yr (Béjar-Pizarro et al., 2010) and approximately 8.5 m of slip has accumulated over the last ~130 years. Although the northern Chile subduction zone failed in "moderate" M_w 7.7 and 8.3 events in 2007 and 2014, these have not fully released the strain accumulated due to plate convergence since 1877 (e.g. Schurr et al., 2014). The seafloor mapping of the northern Chilean subduction zone, for which bathymetry data obtained during cruise SO244 Legs I and II were merged with earlier data sets of RV SONNE and RV METEOR as well as international cruises off Chile, documents a concise fault pattern (Fig. 3.1), with pronounced bending-related normal faulting seaward of the trench. Re-activated spreading fabric overprints the morphology, which modulates the lower slope topography of the upper plate (Geersen et al., 2018). Landward to the trench and the deformation front, a small active frontal prism of 5-10 km width lies adjacent to the lower slope. Normal faulting is widely observed on the middle slope and has been attributed to subduction erosion. The water depth in our three working areas increases from 2800 m to over 5300 m and thus provides an optimal depth distribution for the microbiological work planned during the cruise.

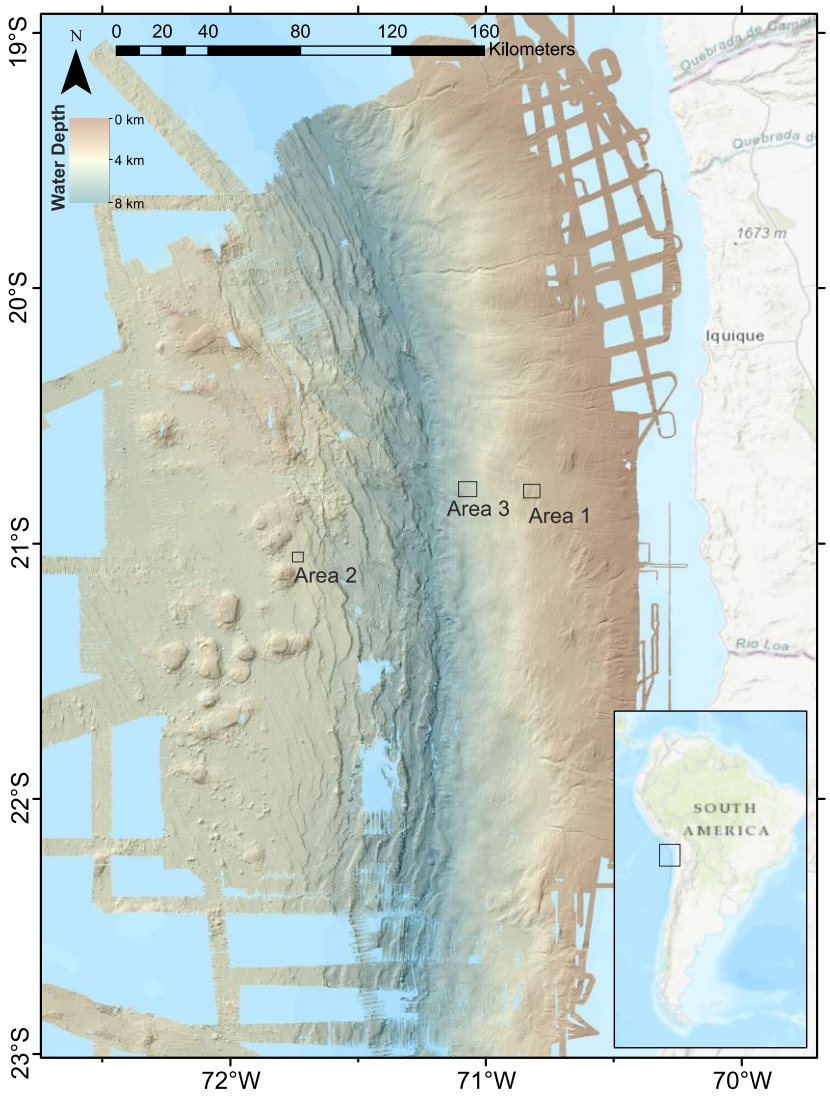

Fig. 3.1 High-resolution bathymetry off northern Chile from multibeam surveys of RV SONNE, RV METEOR and international vessels.

During the MGL16010 cruise of the U.S. research vessel RV Marcus G. Langseth, reflection seismic measurements were made using a 15-km streamer, flanked by ocean bottom seismometer deployments (Petersen et al., 2021). Rupture during the 2014 Iquique event terminated at app. 15 km depth under the mid-continental slope and did not propagate updip to the trench. The rupture area is characterized by the absence of plate boundary reflectivity as resolved in the MGL16010 seismic data (Fig. 3.2). This suggests low fluid pressure that results in stress accumulation and thus controls the extent of earthquake rupture (Ma et al., 2022).

The multichannel seismic (MCS) data show in high precision the top of the dipping oceanic plate beneath and north of the SO288 COMBO project work area, providing an excellent information base for our investigations. A depth-migrated section in the vicinity of the work area tracks the dipping plate to a depth of about 17 km and thus encompasses the location of the GeoSEA array in AREA1 and AREA2 above. The data were merged with earthquake records to resolve possible relationships between the structure of the upper plate and seismic activity (Petersen et al., 2021).

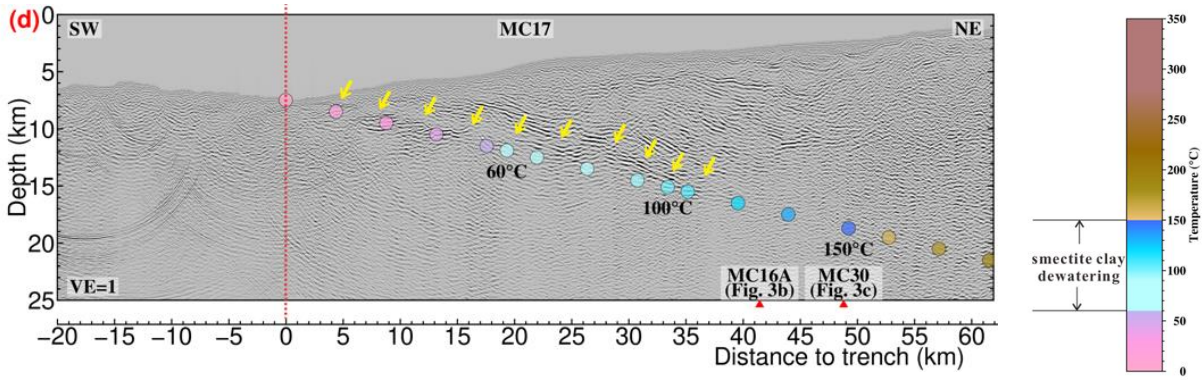

Fig. 3.2 Pre-stack depth migrated section of seismic profile MC17 acquired during cruise MGL16010 of RV Langseth. Yellow arrows indicate the coherent plate boundary reflection. The vertical red dashed line denotes the location of the deformation front. Temperatures are shown as colored dots. The approximate depth range of smectite clay dehydration corresponds to the temperature range 60°-150°C (from Ma et al., 2022).

The GeoSEA array (Lange et al., 2019; Petersen et al., 2019) was installed in the forearc area around 21°S (south of the Iquique earthquake rupture zone) in two networks on the lower and middle slope of the marine forearc, because it is here above the updip limit of the seismogenic zone that the largest deformation is expected (Wang et al., 2012) due to the episodic loading at the trench. An additional network was installed on the outer rise seaward of the trench (Kopp et al., 2015). The deployment areas for the GeoSEA networks were chosen based on the following criteria: (1) water depth between 2000 m and 6000 m, (2) little to no sediment cover and no turbidite channels or evidence for mass wasting events, (3) fault scarps not exceeding 100 m height, (4) evidence for active deformation. Furthermore, the networks should cover the middle and lower slope as well as the outer rise.

Working **AREA1** is located on the middle slope of the continental margin in water depth between 2600-2860 m. An area of approximately 35 km^2 was mapped during Leg I of SO244 using the AUV ABYSS of GEOMAR focusing on a westward dipping normal fault. Several adjacent faults are present, some of which terminate in an undisturbed sediment pond and show

little evidence for recent activity. The main targeted fault is characterized by abundant mass wasting features generally not exceeding lengths of ~80 m across.

AREA2 is located on the outer rise of the Nazca plate about 100 km west of AREA1 and encompasses approximately 17 km^2. Two eastward dipping scarps are the dominant features in the area, which are interpreted to be normal faults that disturb the inherited volcanic features. The overall appearance of AREA2 is generally much smoother compared to AREA1, suggesting a drape of little disturbed sediment. The main target here is to measure the extension across bending-related trench-parallel normal faults in water depth between 4030-4100 m.

AREA3 is positioned on the lower continental plate at water depth exceeding 5000 m. The areal extent of the region is approximately 35 km^2, located approximately 10 km east of the trench. The region is characterized by numerous ridges trending in a NW-SE direction of 140° with heights of up to 500 m and slopes exceeding 15°. A number of flat terraces and peaks are identified in the area, which were used for the installation of the GeoSEA tripods. The main target in this complex area is to measure diffuse strain over long baselines (Fig. 3.3).

3.2 Aims of the Cruise

Cruise SO288-COMBO focuses on the de-installation and recovery of the GeoSEA array off northern Chile. The seafloor geodetic station array was installed at three locations on the Chilean continental slope and the oceanic plate seaward of the deep-sea trench in 2015 during cruise SO244. All three arrays in principle measure the change in the position of a set of points as a function of time (e.g. interseismic creep or the displacement due to an earthquake), thus identifying ‚deformation hotspots' on the seafloor, which then need to be linked to defined geological features. This requires high-frequency seismic profiling to complement the punctual observations of the mm- to cm-scale displacement achieved through the geodetic surveying. This approach is instrumental to interpret the results of the seafloor geodetic survey, and allow inferences regarding the active tectonics of a larger area than the point locations covered by the geodesy. At the end of the active monitoring phase, the instruments including the data loggers are to be recovered. This work will be flanked by seismic surveys. While the seafloor morphology in the area of the three networks is sufficiently known from high-resolution AUV mapping carried out during SO244 Leg I, information on subsurface structures, significantly also on possibly active tectonic faults, is still missing. These are to be detected by means of high-resolution multichannel profiling using GI-guns and a 175 m long streamer. Information on the seismic velocity structure and thus on the structure of the bedrock will be obtained from wide-angle seismic surveying employing ocean bottom seismometers (OBS). This work will be complemented by visual seafloor surveys (ROV camera). The overall goal of the project is to be able to evaluate the geodetic signals recorded over a period of several years differentiated by their origin, depending on the degree of coupling or creep of interseismic type, as well as the distribution of deformation at the plate boundary and within the upper plate. The mechanisms of seafloor deformation are a fundamental unresolved issue in seismology, as it has a direct influence on seismogenesis and thus on the hazard potential of plate boundaries. The seafloor geodetic measurements focus on the three array locations (Fig. 3.1) which were chosen with the aim to address the following specific scientific targets:

- In AREA1, the targeted baselines across a set of westward dipping normal faults aim to

yield information on trench perpendicular motion as well as any possible strike-slip component resulting from slip partitioning. This information is important to validate the tectonic source of possible geodetic signals.

- The main target in AREA2 is to measure the extension across bending-related trench-parallel normal faults in water depths between 4030-4100 m. We aim to quantify the rate of fault motion by measuring the extent across a plate-bending related normal fault using the geodetic array in AREA2. In addition, ground-truthing by a ROV dive targets possible relics of recent fault movement.
- The principal aim in the tectonically complex AREA3 is to measure diffuse strain over long baselines (Fig. 3.3). In order to separate motion on upper plate faults from elastic strain build-up originating from the plate interface thrust, a 'spider web' layout of the array was chosen to cover a maximum area. Detailed 2D seismic profiling above the geodetic array aims to image possible upper plate faults.

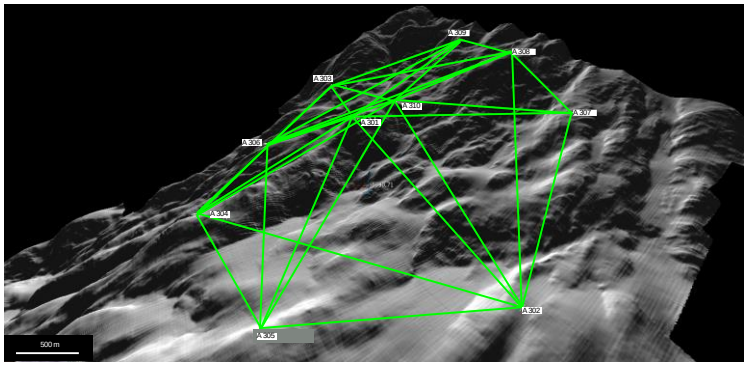

Fig. 3.3 Layout and modeled baselines in AREA3 on the lower slope of the Chilean continental margin in water depth ~5200 m. Green lines are expected baselines between the 10 GeoSEA stations.

3.3 Agenda of the Cruise

A total of 23 GeoSEA transponder tripods were recovered during an intensive dive program of the remotely operated vehicle KIEL ROV 6000. We performed nine dives in water depth ranging from 2700 m to 5300 m. In addition, a seismic program was completed encompassing 988 profile km of multichannel streamer seismics and 181 km of refraction profiling using ocean bottom seismometers. A seafloor bathymetry survey covering 23.200 km^2 on the outer rise of the Nazca plate was conducted while ship operations were reduced to a minimum for nine days due to confirmed COVID-19 infections on board. In addition, seafloor mapping offshore northern-central Chile covering 24.500 km^2 of the forearc was accomplished. The geophysical program was complemented by biogeochemical and microbiological studies encompassing a total of 19 CTD casts and 2 deployments of the snow catcher as well as 2 deployments of the *in situ* incubator.

A cruise plan showing the the route of the ship is provided in Fig. 3.4. A compilation of the regional bathymetry is shown in Fig. 3.1. The ship's station log is in Chapter 6. Measures to ensure responsible marine research and mitigation procedures are described in section 5.4. The scientific objectives of the cruise were achieved despite the delayed start of the work program due to a COVID-19 outbreak on board. Due to time limitations, OBS refraction seismic surveys could only be carried out in two of the expedition's three main survey areas. Except for the bathymetric survey, the geophysical and geodetic work focused on the three working areas offshore Iquique in northern Chile. Also, the biogeochemical and microbiological samples were acquired here.

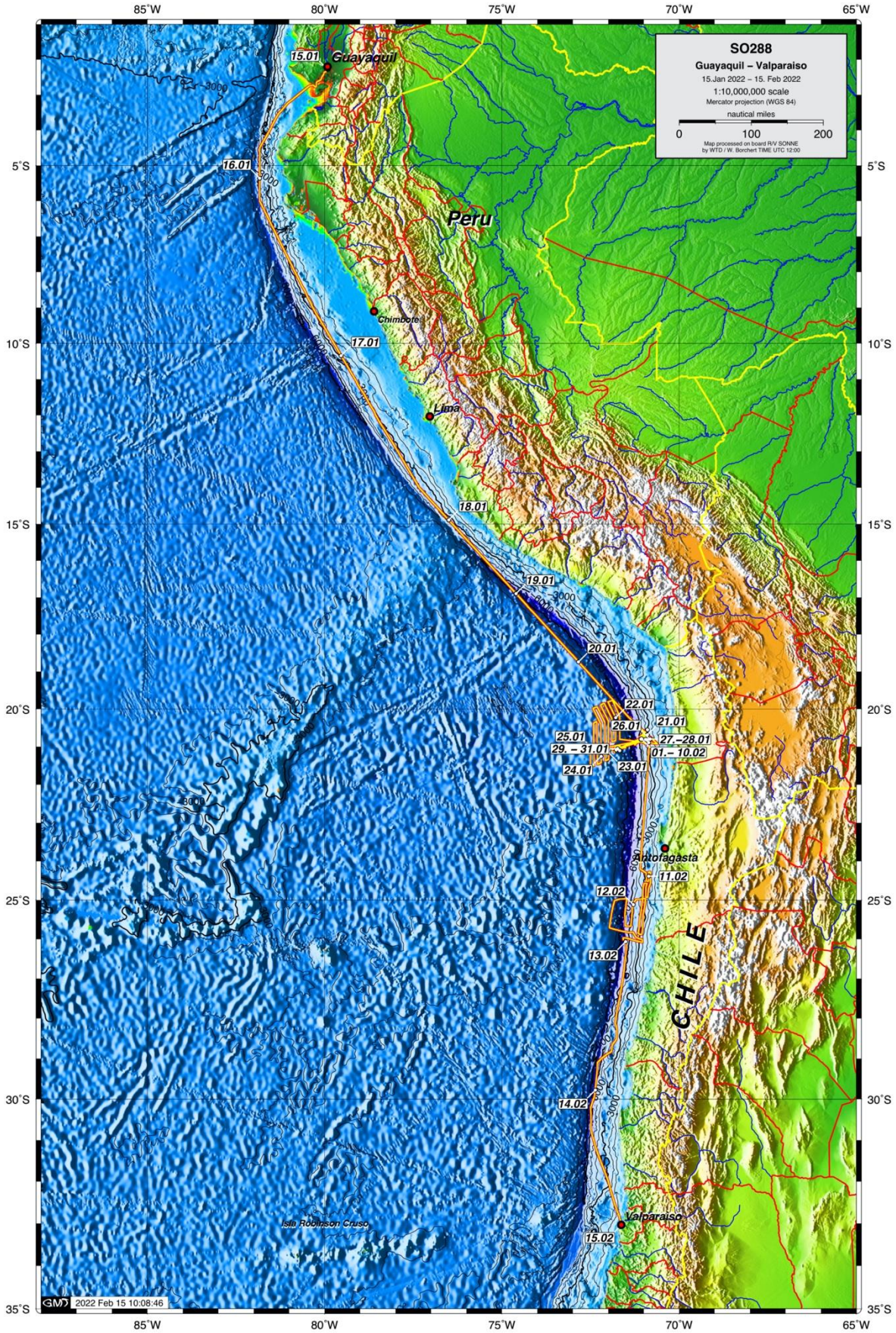

Fig. 3.4 Track chart of R/V SONNE Cruise SO288. Bathymetry from Smith and Sandwell (1997). Three working areas offshore Iquique were the focus of this cruise. Additional multibeam seafloor mapping in uncharted areas between 24°-25.5°S was achieved.

AREA1 was the deployment site of eight seafloor geodetic transponders of the GeoSEA array, which were placed in pairs of two transponders each spaced at a distance of approximately 600 m. The next pair was positioned ~850 m away, roughly following a W-E trend on the middle continental slope. All eight transponders were recovered from the site and 10 CTD casts as well as two deployments of the Marine Snow Catcher (MSC) and one deployment of the *in-situ* incubator (ISMI) were accomplished here.

AREA2 is situated on the outer rise of the oceanic Nazca plate where five transponders were recovered after their initial deployment in late 2015. These transponders had been positioned on both sides of a large normal fault, spaced between 200 m and 800 m apart. In addition, 2D streamer seismic reflection profiles spaced at close distance and 8 nm long were completed here, imaging the subsurface structure which is dominated by the plate-bending related normal faulting. Four CTD casts complemented the data acquisition.

AREA3 is the largest and deepest working area, at a water depth of about 5200 m. A total of 10 GeoSEA stations were recovered from this working area, which was also covered by densely spaced seismic reflection profiles as well as a refraction seismic line shot over 6 ocean bottom seismometers. An *in-situ* incubator experiment was performed here in addition to five CTD casts.

4 Narrative of the Cruise

On Saturday, 15 January 2022 at 13:00 local time (UTC-5) RV SONNE departed from the CONECTON terminal in the port of Guayaquil (Ecuador). The previous days in port were used for final preparations in the laboratories and the mobilization of the remotely operated vehicle (ROV) Kiel 6000 and the seismic equipment, as well as for a COVID-19 PCR screening of the crew, including all 26 scientists. After the 3.5h passage through the Rio Guayas we reached the Pacific Ocean in calm conditions and started the transit south towards our working area in the EEZ of Chile. The scientists used the transit time to finish lab preparations and set up equipment.

Between 17 – 19 January 2022 five cruise participants (2 scientific crew members, 3 ship crew members) were tested positive for COVID-19 and were isolated in their single cabins in accordance with the 'Outbreak Management Plan' guidelines for the current research cruise (OMP-SO288). All individuals except for one person showed no symptoms. Daily antigen tests were performed on all individuals on board for the following 7 days. In addition, containment measures (cohorting the scientific team as well as the crew) took effect: Cessation of all work not necessary for ship operation, prohibition of off-duty meetings, tightening of the mask requirement (only FFP2 masks are to be used), fixed assignment of seats at individual tables in the mess hall as well as expansion to the conference room, closure of the bridge to personnel not on watch as well as closure of the recreation rooms, cessation of cabin cleaning by ship personnel. Official meetings are conducted via video conference, for which a SONNE-internal video client was installed. During this time, the SONNE was close to the coast of Peru, so that in the event of serious symptoms of the disease, it would have been possible to disembark participants quickly at any time.

In order to gain control over the further infection and to prevent all unnecessary movements on board, the planned research work was interrupted for 7 days, combined with daily antigen tests. This measure of 'ship's own quarantine' was essential in order to prevent an interruption of

the voyage as well as to continue to enable the implementation of the research program. There is a consensual desire among both the crew and the scientific team to continue the cruise and to carry out the planned research work.

On Jan. 21, 2022, we reached our work area off the coast of northern Chile the nearest ports in Arica and Iquique can be reached at short notice. began a program of high-resolution mapping of the previously unmapped northern flank of the Iquique Ridge. This work is easily accomplished under the strict hygiene constraints, as only one person is required to be in the hydroacoustics lab at a time, and watch handovers are not direct, but are staggered by 15 minutes so that watchstanders do not encounter each other.

Between Jan. 20 – Jan. 23, 2022, no new infections were confirmed, which was corroborated by a ship-wide PCR screening on Jan, 24-25, 2022, so that instrument deployment could commence in the afternoon of Jan. 25, 2022. The mapping survey was terminated and three CTD stations were conducted in working AREA1, of which the first was also used for a deep-sea test of the ocean bottom seismometer releasers. At 08:00 on Jan. 26, 2022 the ROV was deployed for its first dive, which lasted until 20:00 on that day. During the dive, three GeoSEA stations (A107, A108 and A106, in that order) were recovered using a dedicated recovery frame. Afterwards, five CTD stations were accomplished. The morning of Jan. 27, 2022 saw the next ROV dive and during the day, we recovered two additional GeoSEA stations (A103, A104) before starting the seismic program. After initiation of the mammal mitigation procedures, two GI guns (3.44 l) and a 175 m long streamer were deployed. Unfortunately, data transmission from the streamer failed shortly thereafter, so that the gear was recovered. Instead, three CTD stations were achieved to collect water samples.

On Jan. 28, 2022 at 08:00, the third ROV dive commenced and by the end of the day, the last three GeoSEA stations from working AREA1 (A101, A102, A105) were safely recovered on deck. During the night, we completed an additional seven CTD stations to collect water samples. Some of the samples were immediately filtered on board and stored frozen or refrigerated for analysis of chemical and biological composition at home in the laboratory. Most of the water was obtained from the deep sea (1500 m) to conduct incubation experiments on the degradation of organic material by heterotrophic microorganisms at in-situ temperature (2°C) and in the dark in the ship's climate laboratories. During the night of Jan. 28, 2022, the Marine Snow Catcher, a large-volume water scoop that collects intact particles and associated microbial communities, and an in situ microbial incubator, which allows determination of microbial activity under hydrostatic in situ pressure conditions, were also deployed.

On Jan. 29, 2022, the last person was released from isolation after a PCR test, so that all five infected persons resumed their regular duties. At the same time and after a 55 nm transit to working AREA2, we recovered the five GeoSEA transponders (A201-A205) on the oceanic Nazca plate seaward of the deep-sea trench, installed in water depths up to 4100 m. The transponders were extracted from the tripods (except A204) by the ROV so that the frames could remain in place and new transponders be re-installed at a later time to record long time series. In the evening, the GI air guns and streamer were launched to image the subsurface structures beneath the tripods. Seismic recording proceeded overnight and without interruption during Jan. 30, 2022 until the early morning of Jan. 31, 2022. During the day, four CTD stations were completed to retrieve water samples from the surface to the deep sea (4000 m) for the study of the vertical distribution of organic matter and microbial activity. A general PCR screening on

Jan. 31, 2022, yielded negative results for everyone on board and brought about the lifting of some of the strict safety and hygiene measures.

After a 45 nm transit in the evening, a total of six ocean bottom seismometers were deployed in working AREA3 until the morning of Feb. 1, 2022, when the ROV was deployed at 08:00h for its fifth dive. Unfortunately, at a water depth of 5100 m, we suddenly and unexpectedly lost all communication and control to the ROV. Rescue operations under these difficult conditions lasted until the late afternoon. The following 36 hrs were dedicated to the seismic program with acquisition of a refraction seismic profile using the G-gun array (portside only, 37.6 l) as a source and a survey of reflection lines shot with the GI-guns. Subsequently, the ocean bottom seismometers were recovered and additional CTD stations and an *in situ* incubator experiment were run during the night of February 04, 2022. During this entire time, the repair work on the ROV was running in parallel. Three fibres in the fibre-optic cable turned out to be malfunctioning, so that the cable had to be truncated.

The ROV could be launched again on 04.02.2022 and recovered three GeoSEA stations (A301, A303, A310) from water depths of more than 5200 m until the evening. An extensive reflection seismic program covering 640 km began in the evening and continued over the next three nights, followed by ROV dives during the day. On 05.02.2022 stations A302 and A305 were recovered by the ROV, following some maintenance work on the vehicle's POSIDONIA systems. The ROV dive on the following day recovered stations A306 and A304. On Jan. 07, 2022 the last three GeoSEA transponders (A309, A308, A307) were recovered, ending the ROV program of SO288. Three CTD casts were accomplished until midnight, followed by the 40 nm transit back to working AREA2, where six OBS were deployed until the morning of Jan 08., 2022. At 07:00h mammal mitigation procedures were started prior to the deployment of the G-gun array. Shooting continued until 18:00h that day, after which we recovered the OBS and started the transit back to working AREA1, where a 20 hr MCS-survey was initiated. On Feb. 10, 2022 at 11:00h we left our study sites offshore northern Chile to head south. PARASOUND and multibeam bathymetry were collected during the transit. On Feb. 11, 2022 at 05:00h we entered an uncharted segment of the marine forearc and commenced a dedicated multibeam survey to gain full coverage of the seafloor map reaching from the outer rise seaward of the deep-sea trench to the upper continental shelf. RV SONNE safely reached the anchorage at Valparaiso on Feb. 15, 2022 at 07:00h, terminating cruise SO288. Throughout the cruise weather conditions were optimal, always calm seas and no rain.

5 Preliminary Results

5.1 Hydroacoustic Survey

(L. Murray-Bergquist[1], M. Riedel[1], M. Kühn[1], D. Lange[1], H. Kopp[1], J. Moegeltoender[1]; S. Kontradowitz[1]; B. Thomas[2]; V. Carillo[3], J. Hormazabal[3])

[1]GEOMAR [2]University of Stuttgart [3]Universidad de Chile

5.1.1 Multibeam Bathymetry

Multibeam bathymetry was recorded once the ship reached Chilean waters, with a safety buffer of a few nautical miles to ensure that data was only recorded within Chilean national waters. Bathymetric recording began Jan. 20, 2022 at around 12:30 UTC, and the first survey ended on

Jan. 25, 2022 around 16:50 UTC. The area covered by this initial survey is shown below in Fig. 5.1.

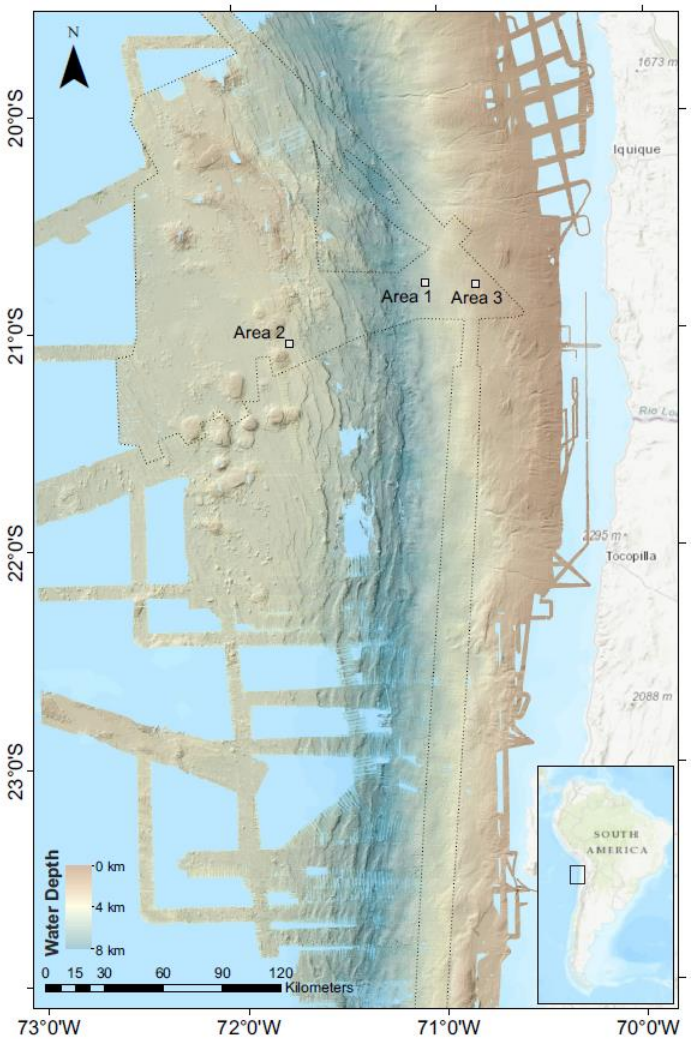

Fig. 5.1 Map showing multibeam bathymetry from Survey 1, study areas are marked.

The system used was the hull-mounted Kongsberg Maritime Simrad EM122 multibeam echo sounder. The system operates at 12 kHz and covers water depths from 20m below the transducers to the full ocean depth. Data acquisition was set to equidistant and multi-ping mode with the FM (chirp modulated) pulse enabled.

The Simrad EM122 system produces 432 beams regardless of swath width. This means that choosing a narrower swath provides a higher beam density and therefore better resolution of the ocean floor compared to a wider swath with larger beam spacing. The beam density also depends on the water depth, the same angle in degrees provides a wider swath with larger beam spacing in deeper water compared to shallower water. The beam angle was set to 65° for the majority of the survey, this was adjusted to 75°, the maximum beam angle, when going over shallower regions or near seamounts, and then readjusted to 65° once the seamount or shallow region had been passed. The survey area, which included study AREAS 1, 2, and 3, covered a total area of about 21,247 km^2, excluding gaps. The focus of this survey was to map the Iquique ridge and some nearby seamounts that were visible on global data sets, but had not been mapped in any detail.

It was initially impossible to record a new sound velocity profile due to an outbreak of COVID-19 onboard, however, a velocity profile from a previous SONNE cruise in the area (SO244) was used for the first few days after which a new profile was recorded.

Once Study AREA1 was reached on Jan. 25, 2022 the bathymetric recording was stopped as the ship remained in approximately the same position to allow for use of the CTD and ROV dives. During the transits between study areas and while the ship was moving for seismic surveys bathymetry was recorded using a beam width of 50° so as to improve the resolution of the survey in these areas. The resulting data quality was very good, although some editing was still necessary. Unfortunately, there are some gaps in the earlier part of the survey where the beam width was not increased next to seamounts and so shallower areas were not reached by the multibeam. Initial processing and manual editing of the multibeam data was carried out onboard in Qimera. The data was then exported in as a floating point geotif grid and plotted in ArcGIS, see Figs. 5.1 and 5.2.

The main goal of the first multibeam survey was to map Iquique ridge and group of seamounts on the oceanic Nazca plate as well as the trench between the Nazca and South American plates. The second survey was conducted further south with focus on filling in data gaps from previous surveys around the Copiapó and the Taltal ridges. The same equipment and procedure were used, the resulting bathymetry is shown below in Fig. 5.2.

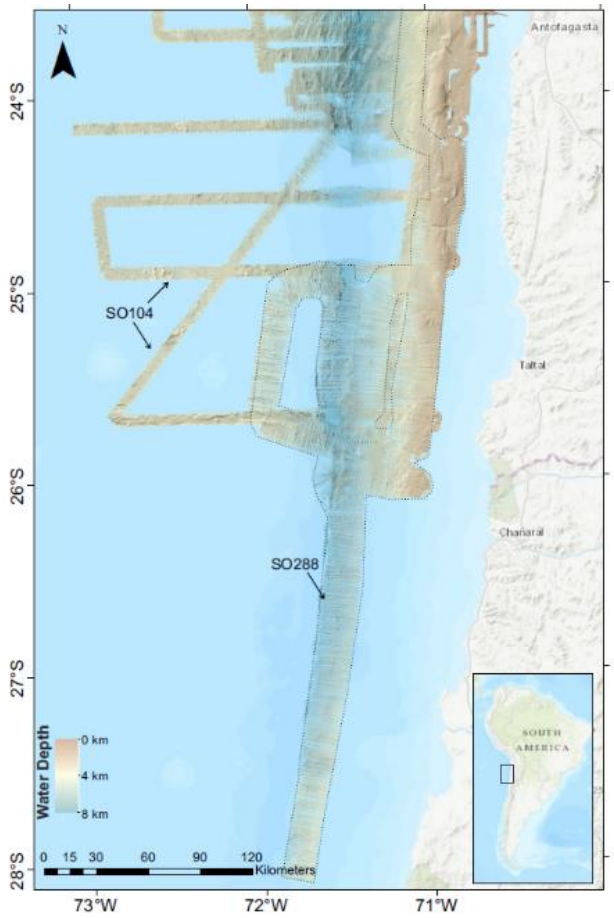

Fig. 5.2 Map showing multibeam bathymetry from Survey 2. The black dashed line separates the new data collected on this cruise (SO288) from data collected on a previous cruise (SO104) in the same area.

5.1.2 PARASOUND

The PARASOUND system was used simultaneously with the multibeam system, and covered the same ship tracks as the multibeam, shown in Figs. 5.1 and 5.2. The main mapping of was carried out from Jan. 20-25, 2022, and more details were filled in during the following days in parallel with work in the three study areas. The multibeam and PARASOUND systems were shut off when the ship was either not moving, or when OBS were being recovered so as not to interfere with the acoustic release commands sent from the vessel.

The PARASOUND data are not high quality. The area was not ideal for PARASOUND due to steep bathymetric gradients caused by seamounts and the subduction trench, and low sediment cover meant that the signal could not penetrate far into the hard seafloor. Examples of the PARASOUND data are shown below in Figs. 5.3 and 5.4.

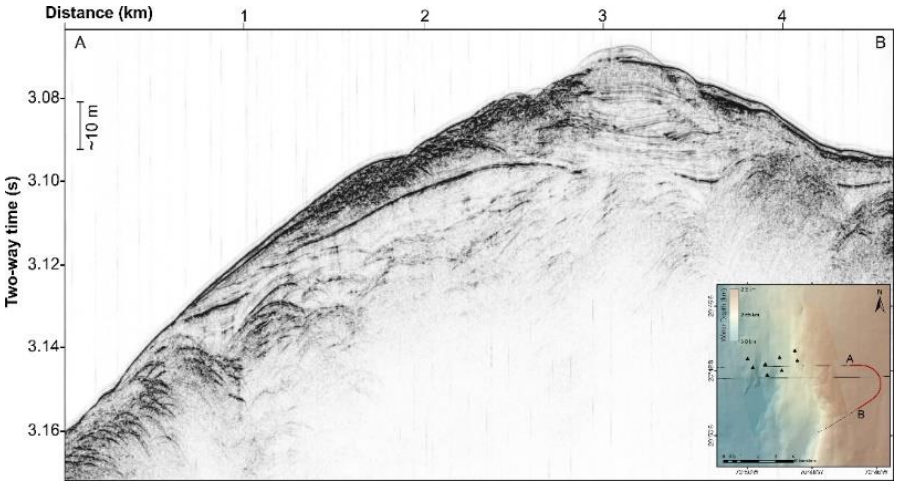

Fig. 5.3 PARASOUND data section from an area on the South American plate collected during the turn of a seismic profile in Study AREA1.

The sediment layer is very thin, near the top of this rise around 3 km on the profile the amount of sediment appears to thicken and a reflector that could be the basement is visible between 1 km and 3 km along the profile.

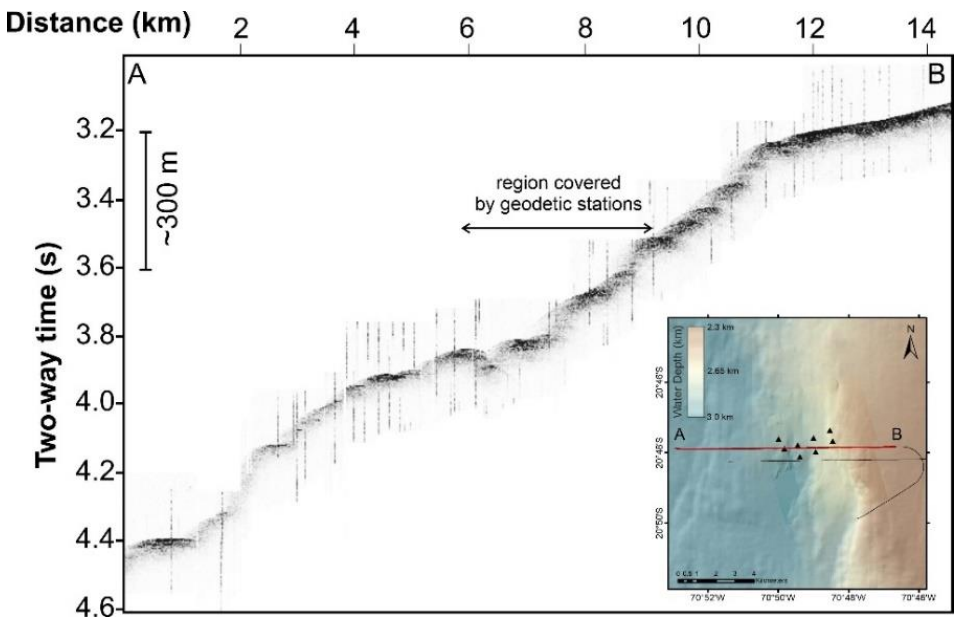

Fig. 5.4 PARASOUND data example from the South American plate crossing the geodetic stations in Study AREA1.

As can be seen in the previous example, the sediment cover is very shallow. Although this is not ideal for PARASOUND, this may have benefitted the geodetic stations which had stable positions on the seafloor.

5.2 Seafloor Geodesy

(D. Lange[1], H. Kopp[1], and Shipboard Scientific Party)

[1]GEOMAR

5.2.1 System Overview and Method

While onshore deformation of faults is monitored using geodetic techniques such as GPS and InSAR, movement of offshore faults remains mostly unknown due to the opacity of water to electromagnetic waves. As a result, we rely on extrapolated observations of GPS land measurements to the marine domain (e.g., Bürgmann and Chadwell, 2014). However, extrapolating onshore observations requires assumptions about crustal properties and fault geometry to determine the locking state of a fault or fault segment. Inferring the slip rate of faults from seismicity includes assumptions about the frictional behaviour of the fault because deformation is known to be partitioned into seismic moment release (micro-seismicity) and aseismic creep (Lange et al., 2014). Our blindness to offshore deformation leads to pivotal debates in science. For instance, the kinematic state of a fault can vary between fully locked to continuously creeping, resulting in a slip accumulation between zero and full displacement along the fault. The fault kinematics is thus determinative of hazard estimates and we are far from the level of knowledge we have on deformation onshore (Bürgmann and Chadwell, 2014).

We use acoustic ranging techniques to measure distance changes of transponders on the seafloor over three years in three geodetic networks to resolve tectonic deformation. The method of acoustic path-ranging between two sites on the seafloor becomes increasingly used in oil exploration (Dunn et al., 2016) and research (McGuire and Collins, 2013; Yamamoto et al., 2019).

The transponders are from Sonardyne (www.sonardyne.com) and measure temperature, inclination, pressure, the sound velocity in the water together with the two-way travel time in-between stations located on the seafloor. Each station either interrogates the other stations of its kind or acts as a replying instrument. Thus, the experiment forms an autonomous intercommunicating network on the seafloor rather than observations at individual positions. The acoustic distance is then calculated from the sound speed in water multiplied by the one-way travel time (Petersen et al., 2019).

Each transponder has an integrated sound-velocity sensor (accuracy 0.030 m/s). However, these sensors showed unexpected offsets and long-term drift of up to 0.5 m/s water speed in the time series during previous deployment in shallow water of ~800 m depth (e.g., Lange et al., 2019). Therefore, we estimate the sound speed in water from temperature and pressure measurements (Leroy et al., 2008), assuming a constant salinity, similar to other path-ranging experiments (Chadwell et al., 1999; McGuire and Collins, 2013). Table 5.1 shows the dependency of the baseline lengths of water parameters.

Baseline change (cm)	Parameter		unit
4.185	Temperature	0.01	°C
1.317	Salinity	0.01	PSU
1.751	Pressure	10	kPa*
*10 kPa = 0.1 bar =m 1 dbar ~ 1 m Water column			

Table 5.1 Dependency of baseline lengths on water parameters for a 750 m long baseline (e.g., 1.500 m acoustic two-way distance).

The three geodetic networks were installed with RV SONNE during cruise SO244-2 between Nov. 27 to Dec. 13, 2015, on the marine forearc and outer rise of the South American subduction system around 21°S (Kopp et al., 2015). The GeoSEA Network consists of autonomous seafloor transponders installed on 4 m high tripods, which were lowered to the seabed on the deep-sea cable of RV SONNE. The array in AREA1 (Fig. 5.5) on the middle continental slope in ~2700 m water depth consists of 8 transponders located in pairs on four topographic ridges. AREA2 (~4000 water depth, Fig. 5.5) is located on the outer rise seaward of the trench, where five stations monitor extension across plate-bending related normal faults seen in the AUV bathymetry. AREA3 is located at water depths ~5200 m on the lower continental slope (Fig. 5.5), consisting of 10 stations to measure potential diffuse strain build-up. Data from all networks and all stations were successfully uploaded with an acoustic modem during cruise MGL1610 of RV Marcus Langseth (December 2016). The last upload was with the Offshore Patrol Vessel Cabo Odger (OPV 84) from the Chilean Navy in June 2018. We could communicate with 20 of the 23 geodetic stations during this cruise. Still, we could only upload parts of the data due to the high energy consumption of marine acoustics from the modem (in ~40 m water depth) to the stations located on the seafloor. All transponders were deinstalled during SO288 with the ROV. The eight stations of AREA1 were deinstalled with the tripods (Section 11.2), all others (except one station in AREA2) without the tripods.

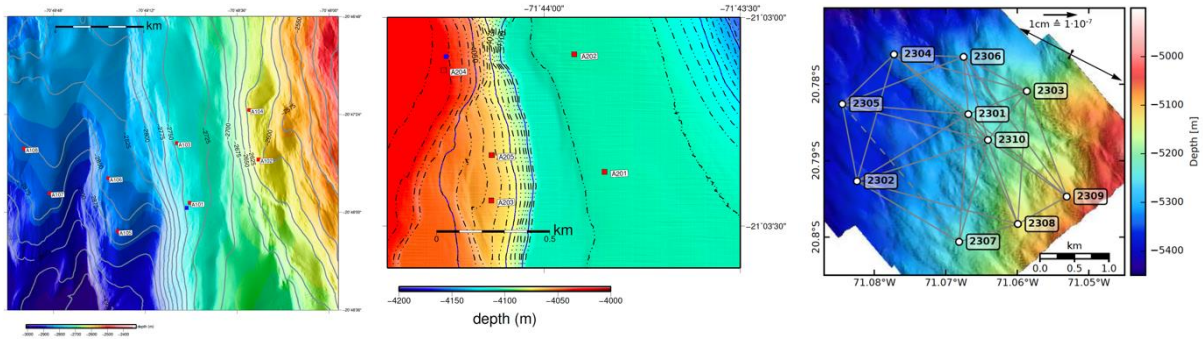

Fig. 5.5 Maps showing the geodetic networks. Left: AREA1, Middle: AREA2, right: AREA3. The bathymetry is from the AUV mapping conducted during SO244, Leg1. The location of the three networks is shown in Fig. 3.1.

5.2.2 Instrument Uptime and Battery Consumption

The main issue regarding instrument uptime is the failure of the high-resolution temperature sensors (red lines in Fig. 5.6). The timing of the temperature sensors appears to be related to the number of measured baselines. For example, in AREA2, baselines were measured every 90 minutes for every responder pair, and logging of all five high-resolution temperature sensors failed before August 2017. In AREA3, the two stations in the center (ID1 & 10) measured to all other transponders, and both failed at the end of 2017.

Figure 5.7 shows the energy consumption of the transponders in AREA1. Battery drain is very linear and similar for all transponders and areas. The battery voltage over time shows the usual behavior for lithium cells, which is a fairly constant battery voltage (13.7V) and a voltage drop at the very end of the lifetime of the batteries (without figure). The transponders stopped working when the battery voltage dropped below 9V. We notice that the transponders stopped

measuring at battery capacity significantly below 100%, suggesting that the battery capacity (given in percent) is overestimated.

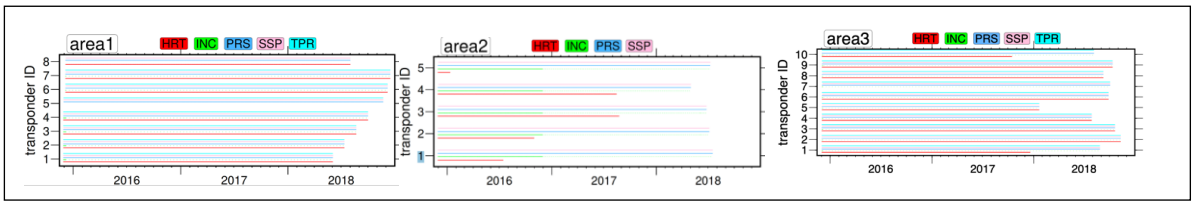

Fig. 5.6 Geodetic data availability for 23 transponders from the three geodetic networks. Station up-time was 100% and was only limited by the lifetime of the lithium batteries (100Ah). HRT: high-resolution temperature; INC: Inclination; PRS: Pressure; SSP: Sound speed sensor, TPR: temperature sensor.

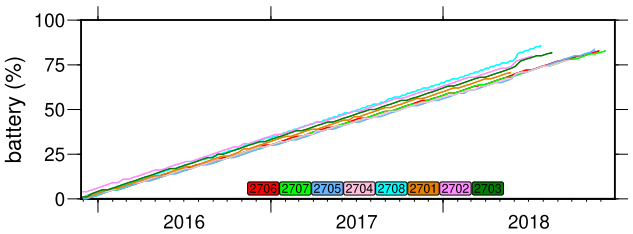

Fig. 5.7 Battery drain for the eight transponders in AREA1.

5.2.3 Seafloor Geodetic Data

5.2.3.1 Inclination

Each transponder measures inclination (pitch and roll) with an accuracy of 0.01°. Since the orientation of the sensors is not known, pitch and roll only relate to the instrument reference frame, which, in turn, can in the future be determined from the ROV videos. Shortly after the installation, all stations have tilt smaller than the amplitude resolution of the inclinometer of 0.01°, which equals to less than 7 mm lateral movement of the top of the 4 m high frames.

We observe very constant values for all transponders during the three years of deployment.

Some settlement effects were measured in the first weeks after installation (Fig. 5.8). After this initial phase, all transponders do not show a tilt signal documenting that the tripods stand stable. The constant inclination is likely related to the very thin sedimentary cover (see Section 5.3 and Figs. 5.3 – 5.4) found during the ROV dives for all three areas and the significant weight of the frames.

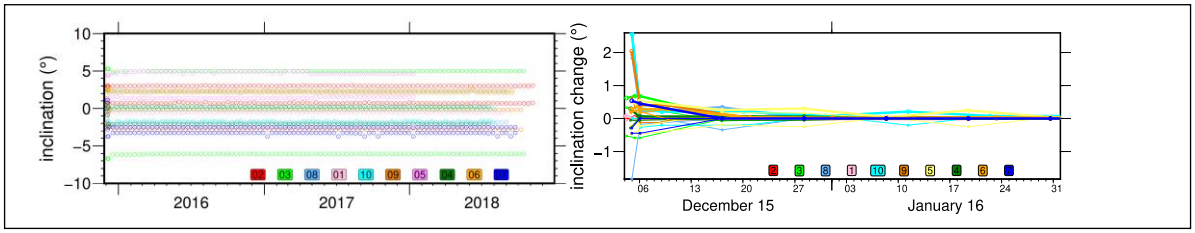

Fig. 5.8 Inclination (pitch and roll, accuracy = 0.01) of all ten transponders in AREA3. Left: Inclination during the three years of measurement. Right: Close-up of the first eight weeks after installation showing settlement, in particular for the first two weeks after installation. Absolute values are difficult to compare. Therefore, zero is set arbitrarily at the beginning of the experiment.

5.2.3.2 Temperature, Pressure, and Sound Speed in Water

In Figure 5.9, we show data examples from AREA3. Besides stations 1 and 10, in AREA3 (Fig. 5.6) all HRT sensors worked, and 42 baselines could be determined. Stations 2306 and 2308 showed an offset in travel times (Fig. 5.9, cyan line) related to the data-download in December 2016 and were not included for this preliminary processing. Pressure (Fig. 5.9) shows a clear settling effect followed by a linear drift of ~0.5kPa/yr with a similar drift for all instruments. This behavior is observed for instruments located in all three areas. The measurement's settling effect is also observed for the travel times (Fig. 5.9, lower-right panel) where travel times directly after the deployment become successively slower, without being compensated by the sound speed.

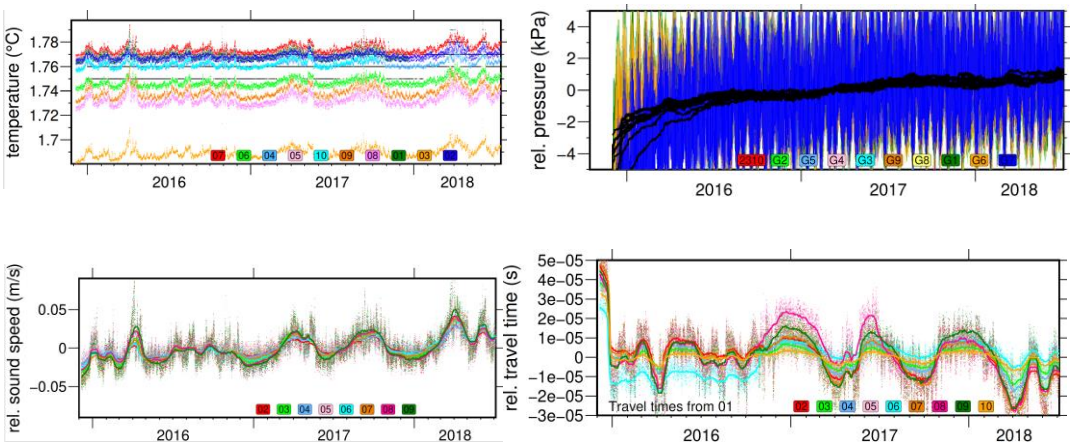

Fig. 5.9 Temperatures (left), pressure (middle) and estimated sound speed (right) for all stations in AREA3. Thick lines indicate two week means. The pressure was set to zero at the beginning of the experiment.

5.2.3.3 Baselines and Strain

The baselines and strain (Fig. 5.10) were calculated using the estimated sound speed in water and the travel times. The sensor settling effect during the first ~2 months of the travel time measurement (Fig. 5.9) directly maps into the baselines and strain estimates and is an artifact. After March 2016, the baselines were all in a corridor of approx. 10 mm width. Considering strain (Fig. 5.9), all baselines are within a corridor of 10^5, indicating the upper bound of resolvable strain.

Baselines of AREA2 work less well since high-resolution temperatures worked only for 1.5 years but look similar to the baselines of AREA3, although only 14 months long. AREA1 still needs some more processing since the baselines still show a significant drift, whose origin needs further investigation.

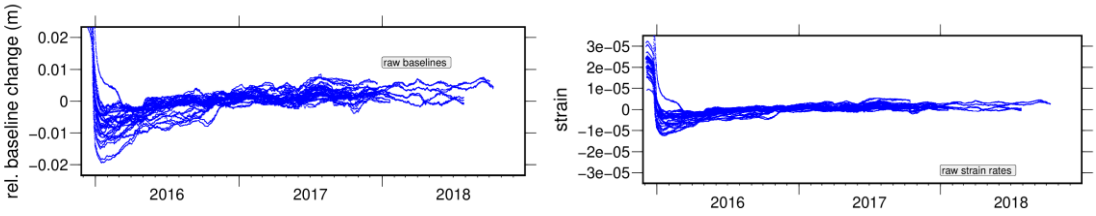

Fig. 5.10 Baseline changes (left) and strain (two week means) estimated for AREA3. Stations 2306 and 2308 are not shown since they had a baseline offset of ~15 mm coinciding with the data upload in Dec. 2016.

5.3 ROV Recovery Operations of the GeoSEA Array

(F. Abegg[1], M. Bodendorfer[1], P. Cuno[1], H. Huusmann[1], T. Matthiessen[1], M. Pieper[1], P. Striewski[1], I. Suck[1])

[1]GEOMAR

ROV KIEL 6000 (Fig. 5.11) is a 6000 m rated deep diving platform manufactured by Schilling Robotics LLC, Davis, USA. It is based on commercially available ROVs, but customized to research demands, e.g. being truly mobile. As a truly versatile system it has been operated from a variety of different national and international research vessels (RV SONNE, N/O l'ATALANTE, RV MARIA S. MERIAN, RV METEOR, RV CELTIC EXPLORER, RRS JAMES COOK and RV POLARSTERN) until today. It is an electrically driven work class ROV of the type QUEST, build No. 7. ROV KIEL 6000 is based at the Helmholtz Centre for Ocean Research Kiel GEOMAR, Germany.

The ROV is equipped with two HD Cameras (AlphaC and Sulis), two SD working cameras (Kongsberg/Imenco), three black and white and one colour observation cameras, seven electric thrusters, one 7-function manipulator ORION and one 5-funtion manipulator RIGMASTER. In addition, a Seabird CTD, a high-definition Kongsberg SONAR and a HOMER distance and direction-finding system are mounted.

Including this cruise, ROV KIEL 6000 has accomplished 319 dives during 26 missions. During SO288, 8 scientific/recovery dives could be accomplished (Tab. 5.2). Maximum diving depth was more than 5300 m, maximum bottom time was 8:16 hours. In total, bottom time accumulated to approximately 41 hours (total dive time approx. 82 hours). One dive (019ROV05) had to be abandoned when the ROV lost communication to the topside control at a depth of 5100 m. After a careful and professional dead vehicle recovery, the evening and next two days were used for fault finding and repair of the vehicle (re-terminating the umbilical).

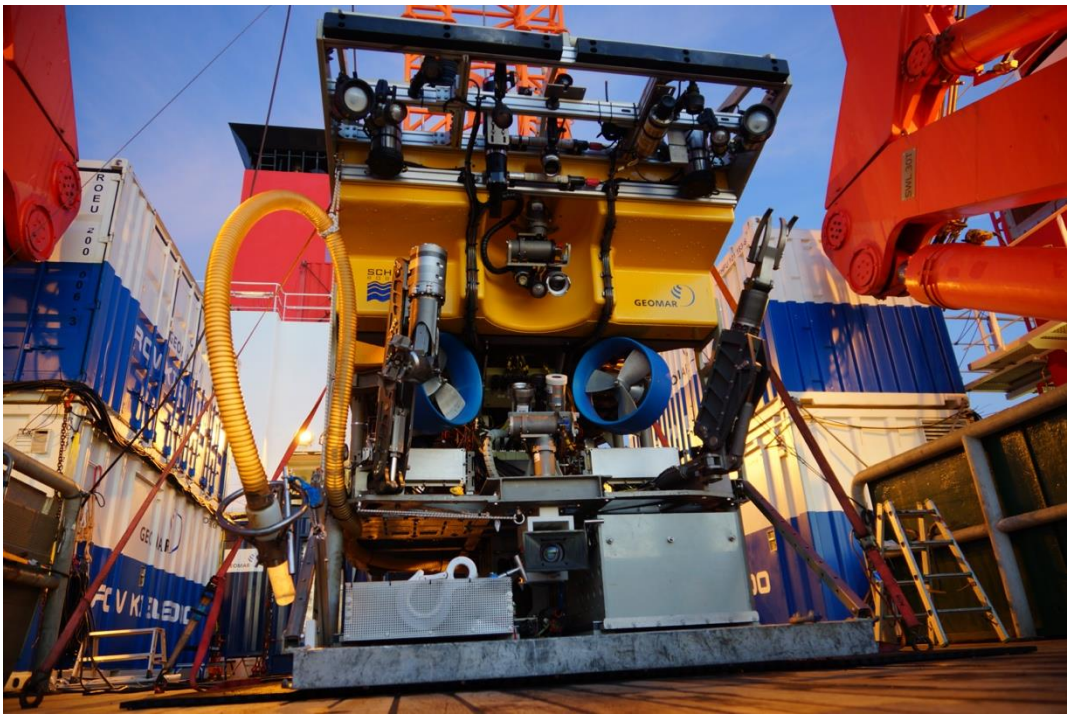

Fig. 5.11

Front view of ROV KIEL 6000

Table 5.2 ROV Station list SO288.

Station Number SO288	Dive No.	Date (UTC)	Time Start (UTC)	At Bottom (UTC)	Off Bottom (UTC)	Time End (UTC)	Location	Depth (m)	ROV Bottom Time
Test	310	15.01.22	Harbour Test Guayaquil., Ecuador						
003ROV01	311	26.01.22	12:30	14:06	22:22	23:55	GeoSEA AREA 1	2850	08:16
005ROV02	312	27.01.22	12:35	13:52	19:41	21:09	GeoSEA AREA 1	2850	05:49
008ROV03	313	28.01.22	12:05	13:20	20:05	21:23	GeoSEA AREA 1	2850	06:45
010ROV04	314	29.01.22	12:03	13:45	18:49	21:00	GeoSEA AREA 2	4100	05:04
019ROV05	315	01.02.22	12:00			21:00	GeoSEA AREA 3	5100	--
029ROV06	316	04.02.22	12:06	14:27	20:24	23:00	GeoSEA AREA 3	5300	05:57
031ROV07	317	05.02.22	16:34	18:58	23:04	01:49	GeoSEA AREA 3	5400	04:06
033ROV08	318	06.02.22	14:45	17:09	19:21	21:47	GeoSEA AREA 3	5400	02:12
035ROV09	319	07.02.22	12:25	14:35	17:29	19:50	GeoSEA AREA 3	5300	02:54
Total: 8 scientific / recovery dives + 1 abandoned dive									**41:03**

5.3.1 ROV Tasks during SO288

During expedition SO288, the main tasks of ROV KIEL 6000 was the search and recovery of seismic transponders (mounted in 4 m high tripods) which had been deployed during expedition SO244 in 2015 (GeoSEA project).

For recovering the transponders together with the tripods, a recovery frame (Fig. 5.12) was deployed on a second wire. This frame is equipped with lights (which can be triggered from aboard by an acoustic signal, a USBL transponder, a HOMER beacon and a spool with a recovery hook. Once a tripod was located (Figs. 5.13 and 5.14), the frame was lowered to the seafloor. The ROV approached the frame, grabbed the hook and engaged the hook in the tripod frame. Hence the frame now "carrying" the tripod including the transponder was lifted and thus recovered.

The second method was to "simply" pull the transponder out of the tripods, store it in the ROV portside drawer and thus recover them.

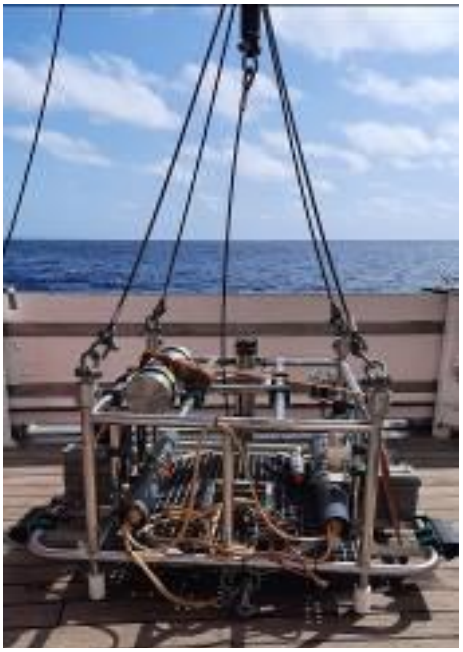

Fig. 5.12 Recovery frame used to retrieve tripods

In 2015, 23 transponders were deployed in three areas (at approx. 2800 m, 4100 and 5200 m depths). During 8 dives, we recovered 9 tripods with transponder, while 14 transponders could be pulled out of the tripods and brought up in the portside drawer of the ROV (Fig. 5.15).

Fig. 5.13 Approaching a tripod with the transponder still mounted.

Fig. 5.14 View of the video monitors in the control room of ROV KIEL 6000 after locating one of the tripods.

Fig. 5.15 ROV with 4 transponders in its portside drawer.

5.4 Seismic Survey

(M. Kühn[1], A. Jegen[1], M. Riedel[1], C. Filbrandt[1], L. Rohde[1], T. Bartels[1], D. Lange[1], H. Kopp[1], L. Murray-Bergquist[1]; J. Moegeltoender[1]; S. Kontradowitz[1]; B. Thomas[2]; V. Carillo[3], J. Hormazabal[3])

[1]GEOMAR

[2]University of Stuttgart

[3]Universidad de Chile

The seismic survey during SO288 encompassed high-resolution streamer profiles in all three GeoSEA working areas as well as two refraction lines which were acquired crossing the layout of the GeoSEA Array in AREA2 and AREA3. The aim of the seismic data acquisition was to detect active structures in the shallow subsurface and link this information to the geodetic signals recorded by the seafloor arrays. As this was a very focused target, we brought only six ocean bottom seismometers and a 175 m GeoEel Streamer, as well as two type of airguns (GI-guns and

a G-gun array, see below). In order to protect marine wildlife during the seismic survey we used airgun ramp-up and visual observation procedures. Ramp-up means the gradual increase in emitted sound levels by systematically turning on the full complement of the array's air guns over a period of time. The intent of ramp-up is to allow sufficient time for animals to leave the immediate vicinity. Visual monitoring of an exclusion zone and adjacent waters is intended to establish and maintain a zone around the sound source that is clear of affected species thereby reducing or eliminating the potential for interference. Exclusion zone means the area of the sea surface within a radius of 750 m surrounding the center of the G-gun array and 500 m for the smaller volume GI-guns. Measures prior to data acquisition included visual monitoring of the exclusion zone and adjacent waters for the absence of sensitive wildlife for at least 60 minutes before initiating ramp-up procedures. Ramp-up was exclusively initiated when visual monitoring of the exclusion zone was possible (i.e. at least 500 m / 750 m visibility and always during daylight hours). The initial shot interval during ramp-up was 2 minutes (GI-guns) to 4 minutes (G-gun) during which the smallest air gun in terms of energy output (dB) and volume (in^3) was active. Additional air guns were gradually activated over a period of at least 20 minutes but no longer than 30 minutes until the desired operating level of the air gun array was obtained. The shot interval was then gradually adjusted to the desired shot point spacing as described below. During acquisition of grid P7000 we experienced a delay of the ramp-up due to sighting of a seal in close vicinity to the air guns. We did not commence ramp-up procedures until 90 minutes after the last sighting of the seal, because the animal was initially so close to the vessel.

5.4.1 Multichannel Streamer Seismic Profiling

High resolution 2D seismic data were acquired to reveal tectonic deformation in the subsurface below the GeoSEA Array stations, covering 987.7 km profile length (Fig. 5.16). All in all, we shot seven seismic surveys with two different acquisition geometries. Survey P1000 was stopped immediately after beginning due to technical problems of the streamer system. Surveys P4000 and P6000 were dedicated to refraction seismic acquisiton and also included streamer data acquisition to cover the uppermost sedimentary layers to basement.

5.4.1.1 Streamer Setup

We used 14 active sections (Geometrics GeoEel streamer segments, each 12.5 m long) with an overall digital streamer length of 175 m for recording the seismic signals. Deck geometries, streamer configuration and seismic gun settings for the 2D survey are illustrated in Fig. X2-X3. The seismic recording unit consists of a tow cable, a 25 m long vibro-stretch section behind the tow cable and the 14 active sections attached behind the stretch zone. The tow cable has a length of 42 m behind the vessel's stern. Each active section contains 8 hydrophones with a group spacing of 1.56 m. Each active streamer section has an analog-to-digital (AD) converter module. Communication between the AD digitizer modules and the recording system in the lab was transmitted via TCP/IP protocol. A repeater was located between the deck cable and the tow cable (Lead-In). The streamer power supply unit managed the power supply and communication between the recording system and the AD digitizer modules. A small buoy was attached to the tail swivel of the 2D streamer.

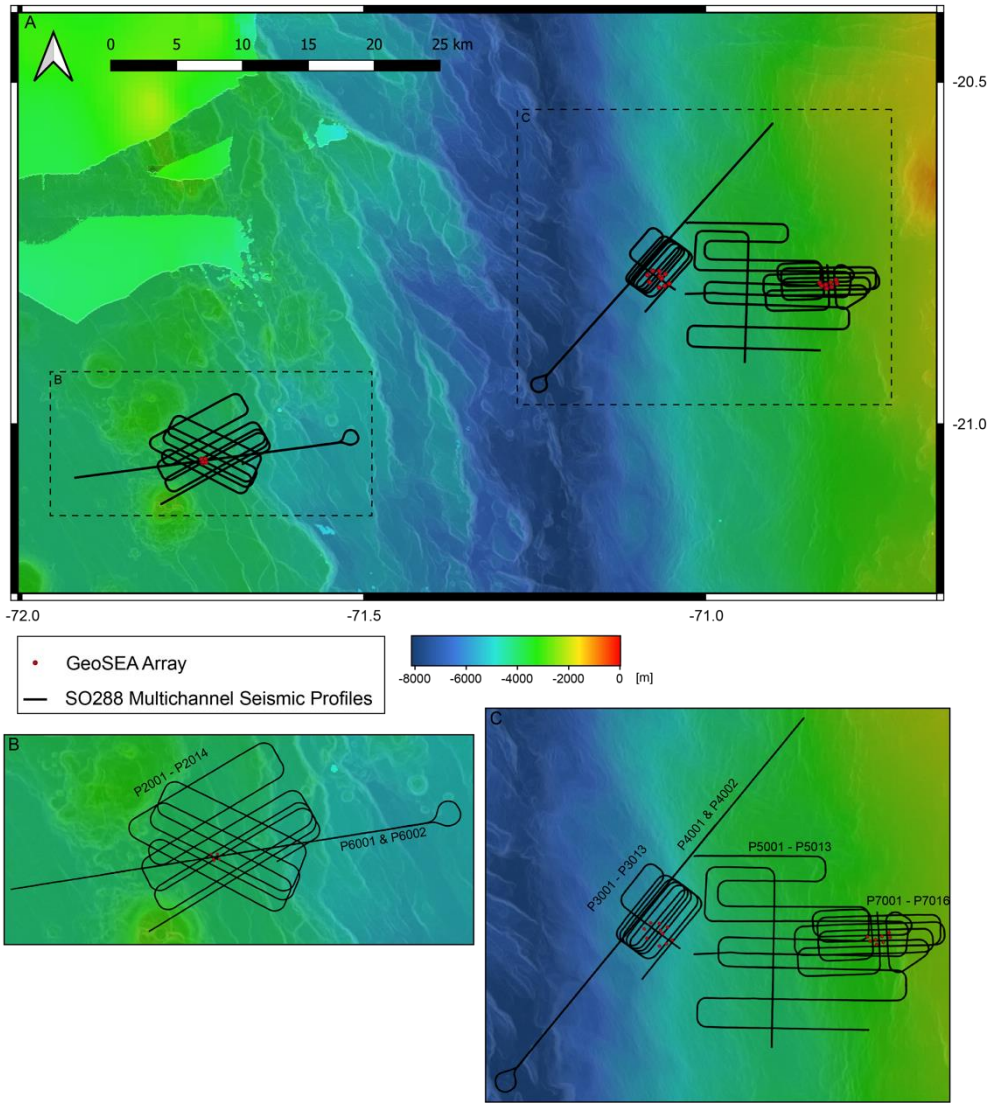

Fig. 5.16 Overview of the multichannel reflection seismic data acquired during SO288 (A). B: Zoom on AREA2. C: Zoom on AREA1 and 3. Background: bathymetry from SO244 and GMRT plotted with slope shading.

Four Bird Remote Units (RUs) were deployed on the streamer during the survey in order to maintain a streamer depth of ~ 2 m. The RUs have adjustable wings that were controlled from the seismic lab. Controller and RUs communicate via communication coils nested within the streamer. A twisted pair wire within the deck cable connects controller and coils. One of the RUs was not connected to an active section, but to a 1.56 m long bird section added to the streamer system (Figs. 5.17 and 5.18), which allows RU communication without containing a hydrophone for recording. This bird section increases the channel spacing at its position to 3.125 m, which has to be considered for geometry calculations.

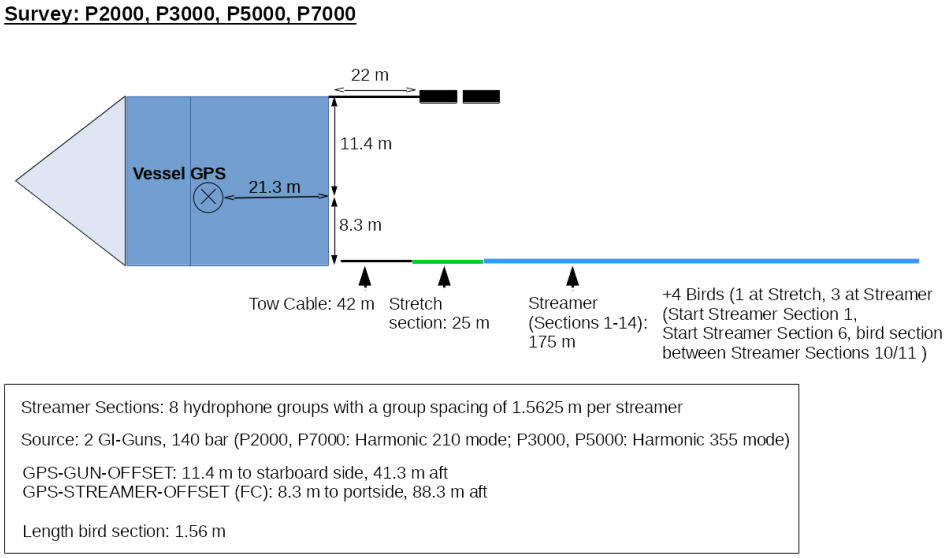

Fig. 5.17 Deck geometry for survey P2000, P3000, P5000 and P7000.

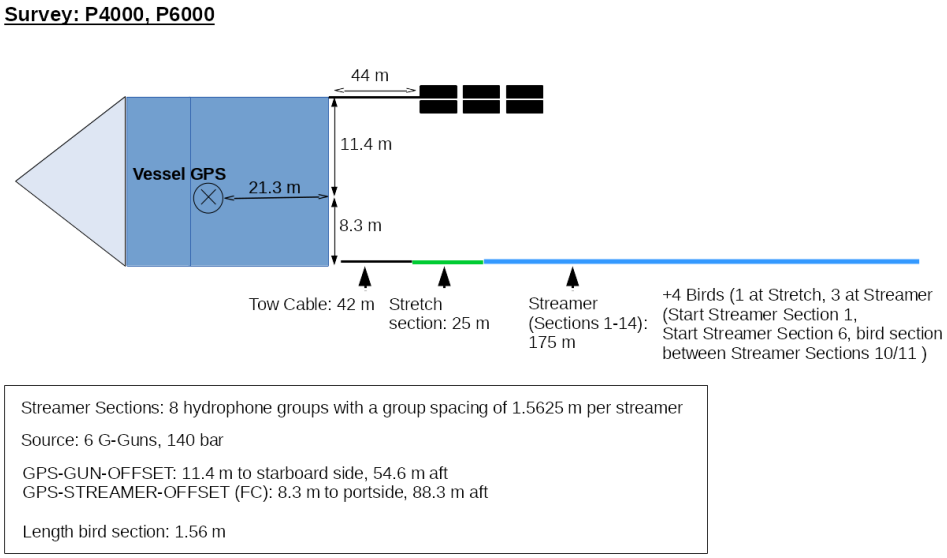

Fig. 5.18 Deck geometry for survey P4000 and P6000.

5.4.1.2 Seismic source: GI-Guns

During the multichannel seismic experiment, two GI-Guns (Generator-Injector Guns) were used as seismic source. Each gun was connected to a stringer by two steel chains 1 m above the gun. Two buoys stabilized the guns in a horizontal position at a water depth of approximately 2 m. The GI guns were operated in Harmonic 210 mode (105 in^3 generator and 105 in^3 injector chamber) during surveys P2000 and P7000. For surveys P3000 and P5000 one GI-Gun was used in Harmonic 355 mode (250 in^3 generator and 105 in^3 injector chamber), while the second GI-Gun was used in Harmonic 210 mode. Unfiltered frequency spectra of one generic shot from surveys P5000, P6000 and P7000 are shown in Figure 5.19. A gun hydrophone provided both the time break and the shape of the near-field signal for permanent monitoring and quality control of the source signal. The injector pulse was triggered with a delay of 55 ms in respect to the generator pulse. This delay value was adopted for an approximate source depth of 2 m and a gun

pressure of 140 bar. Detailed information on the G-Gun Array that was used for the refraction seismic experiments (P4000 and P6000) can be found in the corresponding section of this report.

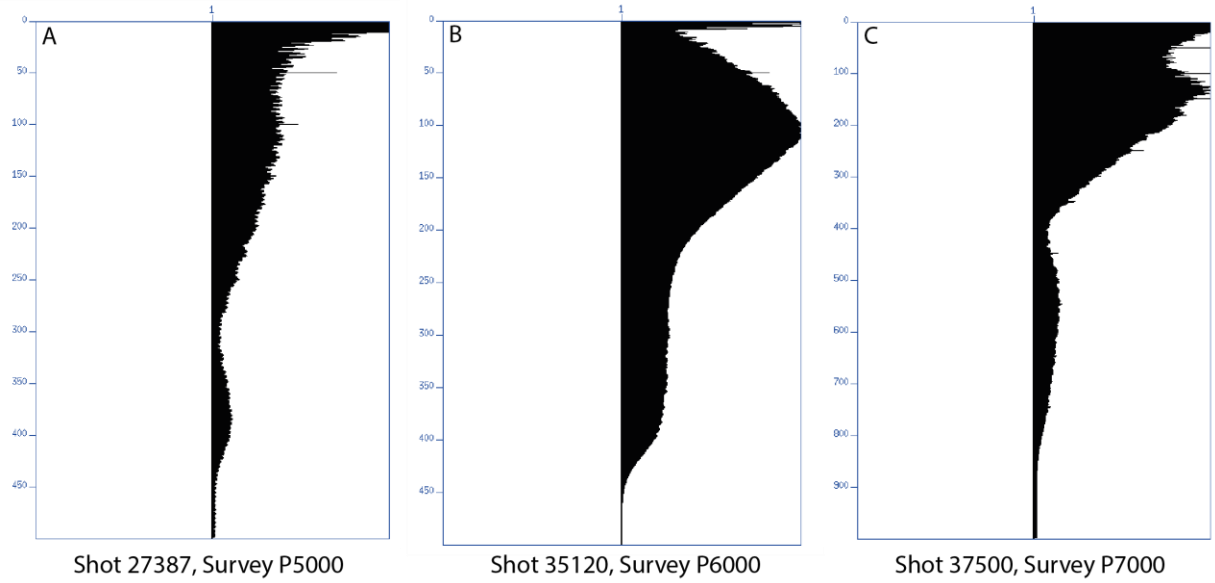

Fig. 5.19 Unfiltered frequency spectra from survey P5000 (A), P6000 (B) and P7000 (C). P5000 was shot with one GI-Gun in Harmonic 210 and one GI-Gun in Harmonic 355 mode. P6000 was shot with the G-Gun Array and P7000 was shot with both GI-Guns in Harmonic 210 mode. Y-Axis: Frequency in Hz.

5.4.1.3 Data Acquisition

Data were recorded with acquisition software provided by Geometrics. The analogue signal was digitized with a sample rate of 1 milliseconds (except for survey P7000 with 0.5 milliseconds sampling rate). The seismic data were recorded as multiplexed SEG-D. One file with all channels within the streamer configuration was generated per shot. The corresponding logged shot file reports shot number and time information contained in an RMC string. The acquisition PC allowed online quality control by displaying shot gathers, a noise window, and the frequency spectrum of each shot. The cycle time of the shots were displayed as well. The vessel's position was simultaneously logged in the RMC string along with logged time and position information with a GPS antenna.

Table 5.3 Acquisition parameters of the multichannel reflection seismic experiments during SO288.

	P2000	P3000	P4000	P5000	P6000	P7000
Shot rate	10 s	12 s	30 s	10 s	30 s	8 s
Recording length	8 s	10 s	14 s	9 s	14 s	7 s
Sample rate	1 ms	1 ms	1 ms	1 ms	1 ms	0.5 ms
Shot mode	Harmonic 210	Harmonic 355 & Harmonic 210	G-Gun Array	Harmonic 355 & Harmonic 210	G-Gun Array	Harmonic 210

5.4.1.4 On-Board Processing

On-board processing included streamer geometry configuration, delay calculations and source and receiver depth control. From the seismic data a delay of -50 ms was evaluated. A receiver or source ghost effect could not be detected in the main frequency range of the surveys (~ 50 – 250 Hz). The source-receiver locations were then binned with a common-midpoint bin spacing of 1.5625 m. Different filter tests were performed and the frequency spectra (see above) were analyzed. Seismic traces were balanced and filtered using a bandpass filter with corner frequencies at 15, 48, 350, 450 Hz (Fig. 5.20). Subsequently, a normal move out correction (with a constant velocity of 1504.00 m/s, derived from a CTD measurement) and stacking were applied. The stack was migrated with a 2D Stolt migration algorithm using a constant velocity model of 1500 m/s.

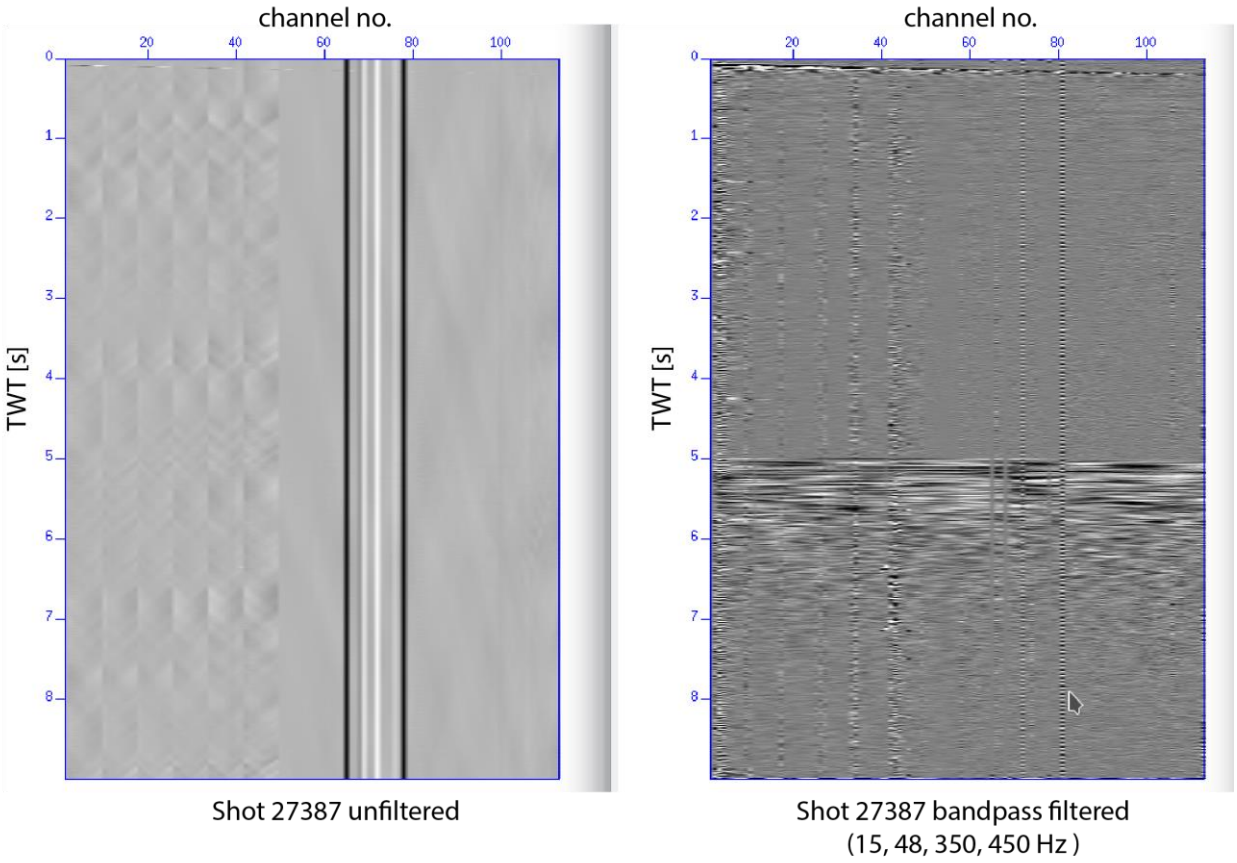

Fig. 5.20 Unfiltered (left) versus filtered (right) shot gather. The unfiltered shot gather image shows low-frequency noise overlying the true reflections starting at ±5 s TWT. In the filtered shot gather reflections are clearly visible and the signal-to-noise ratio is highly improved.

5.4.1.5 Preliminary results

In total, we acquired 987.7 km of seismic profiles. The data are of good quality and provide insights into the geological and tectonic setup of each research area. We show one example of a stacked and migrated seismic profile from each research area in the following sub-sections.

AREA1

The multichannel reflection seismic sections shot over AREA1 (Fig. 5.21) show a continuous and coherent seafloor reflection, indicating that the geometry calculations for gun and streamer

channels are acurate and that no ghost effect is obscurring the reflected seismic signal. The seafloor and sub-seafloor domains show a high degree of deformation, expressed in active extensional faulting and folds. Only a thin sedimentary apron covers the continental basement; most sediment is highly compacted. The GeoSEA stations were placed across a set of bathymetric lineations and the seismic image reveals these to be surface traces of active faults.

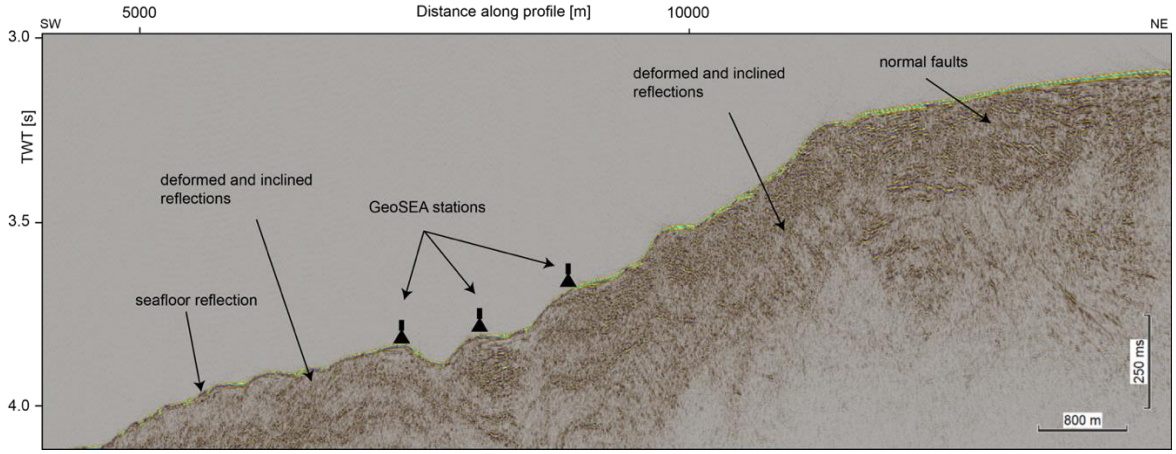

Fig. 5.21 Reflection seismic profile P7003, AREA1, showing large scale deformation and fault patterns.

AREA2

The multichannel reflection seismic sections shot over AREA2 are of good quality, though some migration artifacts manifested as coherent, horizontal noise above the seafloor reflection remain, indicating an inappropriate migration velocity model (Fig. 5.22). However, the original seafloor reflection is clear and sharp, implying acurate geometry calculations. Below the seafloor reflection at 5.39 s TWT in the southwestern part of the profile, a ~ 0.1 s TWT thick package of hemi-pelagic / pelagic sediment is visible, indicated by continuous, coherent and parallel reflections. Below these sediments, at 5.5 s TWT, a strong coherent reflection marks the impedance contrast between the sediment and the oceanic basement. Trench parallel plate-bending related normal faults (black stippled lines) reach offsets of ~0.1 s TWT. Towards the NE of the profile, a tilted basement block is recognized underneath the horizontally stratified sediment cover.

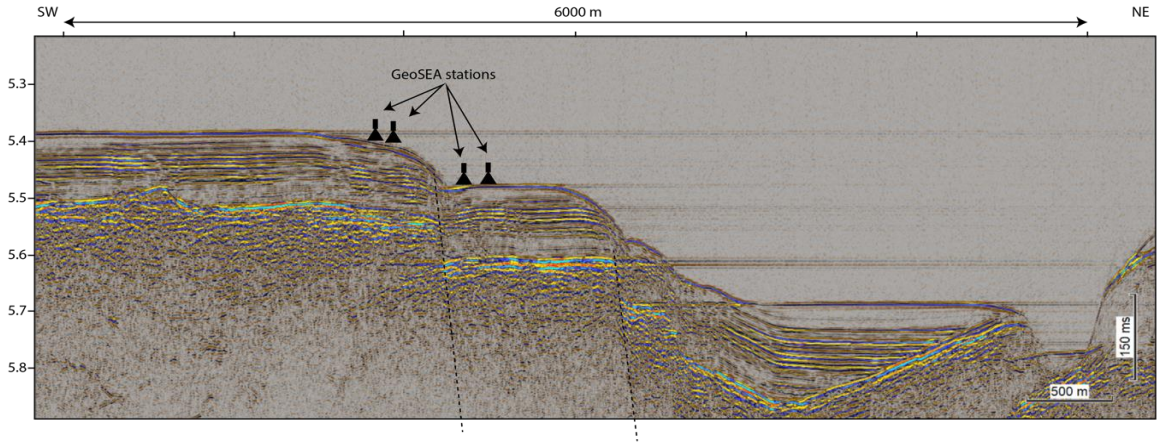

Fig. 5.22 Reflection seismic profile P2002, AREA2, showing the deformation of the Nazca plate before subduction.

AREA3

Figure 5.23 shows a seismic profile shot across the GeoSEA array on the lower continental slope, approximately 10 km east of the deformation front. A sharp seafloor reflection is underlain by incoherent and discontinous reflections below. The seismic profiles in this area require post-cruise reprocessing with an adequate velocity model to increase the imaging of subsurficial structures. The almost opaque character of the seismic data is indicative of highly disturbed, compressed and solidified material. The seismic section suggests that the GeoSEA stations were placed on bedrock with neglectable soft sediment, so that the geodetic signals from the array will document the tectonic deformation pattern of the upper plate instead of sediment migration.

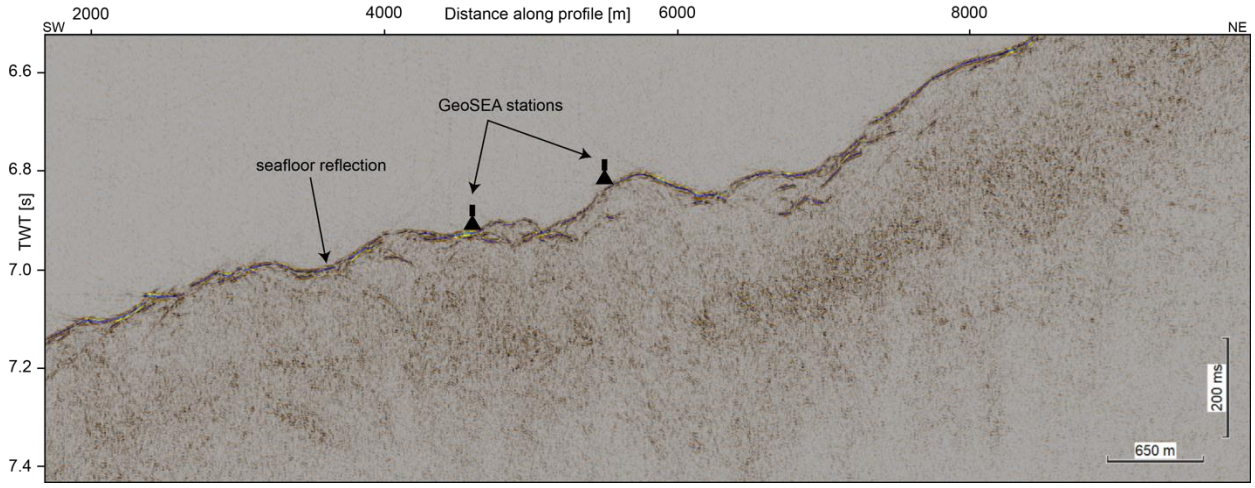

Fig. 5.23 Reflection seismic profile P3008, AREA3.

5.4.2 Refraction Seismic Profiling

5.4.2.1 Ocean Bottom Seismometer

Six of GEOMAR's short-period Ocean Bottom Seismometer (OBS) instruments were deployed and recovered at both of the OBS survey locations. All of the deployed OBS where of the type OBS-2002, the design of which was based on experiences gained by the work with the GEOMAR Ocean Bottom Hydrophone (OBH; Flueh and Bialas 1996) and the GEOMAR Ocean Bottom Seismometer (OBS, Bialas and Flueh, 1999). The used OBS systems record the emitted seismic wavefield by measuring both the acoustic pressure in the water column and the local ground displacement, which are measured by a mounted hydrophone (HTI-01-PCA hydrophones; High Tech Inc.) and a 4.5 Hz three-component seismometer (K.U.M, modified after Tim Owen (Cambridge)). GEOLOG recorders, which were developed at GEOMAR were used to record the measured data with a sampling rate of 150 Hz. For the recording, an additional reduced power source, as well as an atomic clock are required to power the recorder and generate an autonomous time signal. The recorder, as well as the power source, the atomic clock and the seismometer are encased in titanium tubes to protect the gear from the substantial ambient pressure down to 6000 m water depth. The OBS possesses a flotation body made of synthetic foam, which produces enough buoyancy to hold the OBS at the sea surface. The buoyancy of the OBS is counteracted by a massive anchor frame (~60 kg), which is attached horizontally to the

bottom of the OBS before deployment and is released when the OBS is to be retrieved. The release is made possible by an acoustic release transponder (the K/MT562; K.U.M GmbH), which disconnects the OBS from the frame, causing the OBS to rotate by 90° and start to ascend to the sea surface, when a specific signal is emitted into the water column. The rotation of the OBS during its ascend is caused by the position of the instrument's centre of mass and procures that the transponder unit of the OBS remains under water and can thus react to emitted range signals enabling its localisation.

5.4.2.2 Seismic Source: G-Gun Array

A G-Gun array produced by Sercel Marine Sources Division and Seismograph Services Inc. was used as seismic source during the data acquisition of the 2 OBS surveys. The array consists of 6 guns, which were set up in 3 clusters with 2x8 litre G-Guns at the outer position that framed either 2x4 litre or 2x6 litre G-Guns which were placed in the inner positions. This gun distribution was chosen because it provides a good primary-to-bubble signal ratio and the total volume of the six guns amounts to 37.6 litres, which should enable significant penetration. Airgun-deployment rails mounted on RV SONNE were used to deploy the G-Gun array on the aft port side of the ship. During data acquisition, the array was towed 40 m behind the ship's stern, where they were triggered 6 m below the sea-surface with 170-280 bar. In order to achieve maximum ray coverage, the G-Gun array was used with a shot interval of 30 s, which roughly translates to a shot point distance of 60 m at 4 kn speed. Similar to the receiver distance, the shot interval was chosen to optimise the prerequisites for a later velocity inversion. A small shot interval increases the ray density, which reduces the ambiguity of a later velocity inversion due to an increased number of crossing ray paths and thus improved spatial resolution.

5.4.2.3 Data Acquisition and Survey Areas

Due to time limitations, OBS refraction seismic surveys could only be carried out in two of the expedition's three main survey areas. The survey areas, in which six OBS-2002 were deployed each (AREA2-3), are marked in Figure 5.24. Refraction seismic surveys were undertaken for later subsurface velocity distribution inversion, the knowledge of which will complement the extensive reflection seismic surveys (Section 5.4.1) and help in the correct imaging of subsurface features such as faults and thus in the interpretation of the GeoSea network data (Section 5.2).

AREA3

A total of six OBS were deployed in AREA3 each spaced 900 m apart (Fig. 5.24A). This receiver distance was chosen, because a compromise was sought between resolving the seismic velocity distribution along the entire length of the GeoSea Array (Section 5.2) and achieving a maximum subsurface resolution. The OBS were overshot twice once from SW-NE and a second time from NE-SW. While the NE-SW transect, which was acquired first was about 36 km long and exceeded the OBS by 19 km towards the southwest and about 12 km towards the northeast, the subsequently acquired SW-NE transect was lengthened by 16 km towards the NE. Such an excess transect length benefits a later velocity inversion, because signals with large receiver-source offset improve the resolution of deep structures. Further, the two-sided data acquisition enables a later quantification of asymmetric ray paths.

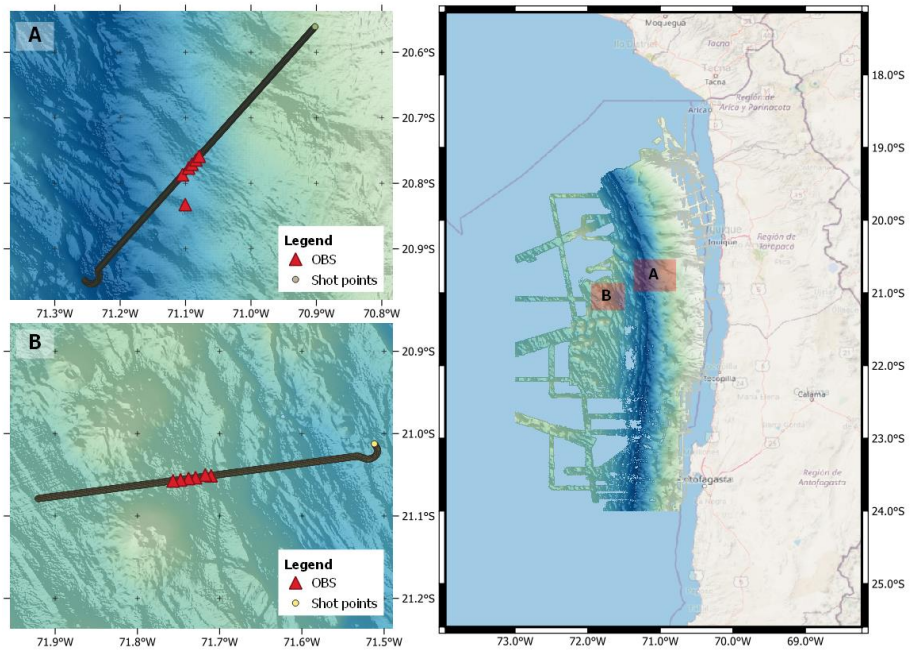

Fig. 5.24 Overview of the general location of the two OBS surveys, complemented by a closeup of AREA3 (A) and AREA2 (B).

All deployed OBS were successfully recovered, though OBS 2 displayed a strong drift during its descend to the seafloor and is offset relative to its planned position by about 5 km. A first sighting of the records conveyed that four OBS successfully recorded the executed seismic survey of which only one showed a larger time drift (OBS33). Two other OBS (OBS31, OBS32) showed issues with the recorder, though we are optimistic to retrieve the data from at least one OBS. The shot gather, which was recorded at OBS 35 during the NE-SW trending measurement of the transect, was extracted and is shown in Figure 5.25A. Even though some noise remains in the shot section both the seabed reflection and a first refraction are visible in the shot gather, despite the preliminary, basic processing that was applied.

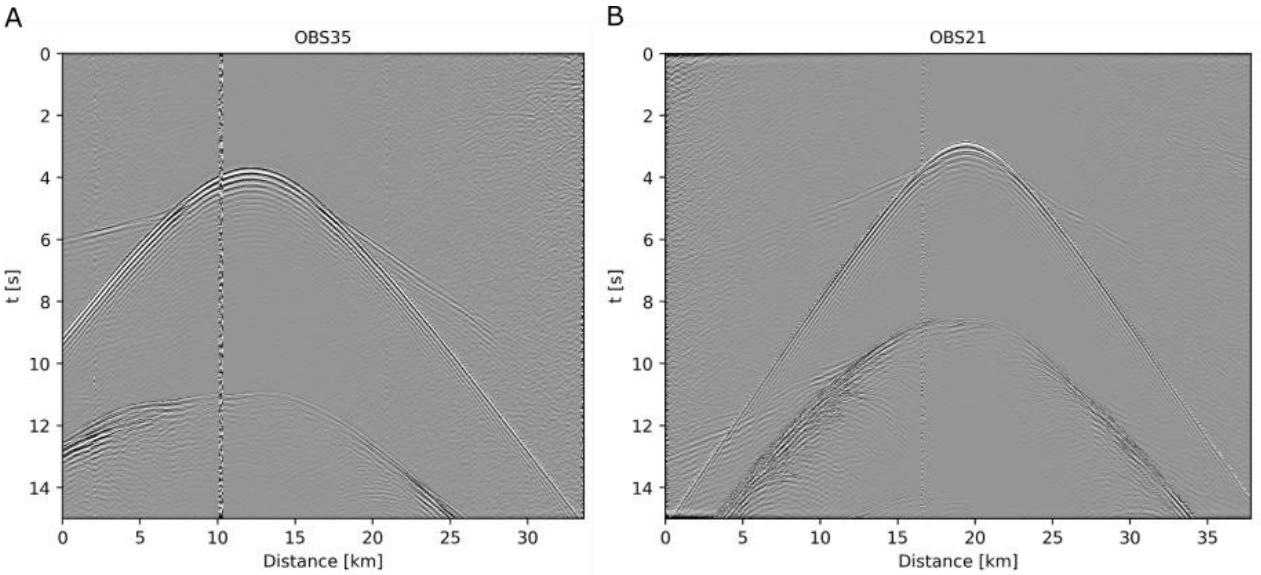

Fig. 5.25 Exemplary data excerpts taken from an OBS of each survey area (A: AREA2, B: AREA3) before relocation of the OBS. The sections were processed with a wide filter (1,4,80,120 Hz), are vertically exaggerated by a factor two and weighted with the 70th percentile for visualization purposes.

AREA2:

The OBS, which were recovered from AREA3 were re-deployed in AREA2, each spaced about 900 m apart (Fig. 5.24B). The station spacing was decided under the same considerations as in AREA3, where a compromise between ray density and OBS survey length was sought. As in AREA3, the transect of AREA2 was shot from both directions, here due to the orientation of the second survey from E-W and W-E. While, the W-E trending transect was shot symmetrically and exceeds the OBS survey by 17.5 km in both directions, the subsequently shot E-W trending transect was shortened by 10 km west of the survey (Fig. 5.24B). All OBS were recovered successfully and data could be downloaded from all six recorders. Further, none of the mounted autonomous clocks showed a larger time drift than 2 ms. The data from OBS21 were exported and visualized. The data appear unnoisy, but show weak amplitudes at larger station offsets in the preliminary section (Fig. 5.25B).

5.5 Biological Oceanography

(K. Becker[1], B. Pontiller[1], R. Flerus[1], A. Engel[1], M. Rosmann[1], C. Amano[2], B. Mähnert[2])

[1]GEOMAR

[2]University of Vienna

The Humboldt Current System is one of the most productive ocean areas in the world. Upwelling of nutrient-rich deep water supports high net primary production, a key process in the global carbon cycle. In general, these areas are highly significant for carbon export via the biological carbon pump, which is an important removal process of CO_2 from the atmosphere. Additionally, the total amount of organic carbon dissolved in the ocean is roughly equivalent to the amount of carbon found in the atmosphere in the form of carbon dioxide. This means that the ocean and in particular the deep ocean represents a vast organic carbon reservoir. Dissolved organic matter (DOM) produced in the surface by algae accumulates in the deep ocean after export and transformation as so-called recalcitrant DOM, i.e. DOM that is difficult to degrade by microbes. However, key aspects involved in the cycling of organic carbon in the deep ocean remains largely unknown and how the fate of the organic carbon will change in the future ocean is uncertain. Thus, the goal of Humboldt Organic Matter Remineralization (HOMER) is the detailed biochemical characterization and turnover of particulate and dissolved organic matter in the water column, in particular in deep, meso- and bathypelagic. To this end, we collected water samples for *state-of-the-art* (micro)biological and chemical analyses as well as for microbial activity measurements. The discrete seawater sampling was combined with onboard incubation with natural bacterial communities to investigate the influence of source, lability, composition, and concentration of organic matter on microbial processes at different temperatures relevant to organic matter turnover in the deep ocean. The effect of pressure on microbial activity an in-situ microbial incubator, which allows determination of microbial activity under hydrostatic in situ pressure conditions, were used during the cruise deployed. Table 1 summarizes the deployment of instruments for our work.

5.5.1 CTD-Rosette System

During SO288, a total of 19 vertical profiles of pressure (P), temperature (T), conductivity (C) and oxygen (O) were recorded. The CTD/O2 profiles ranged from the surface to 5000 m depth. We used the ship's CTD system attached to the water sampler carousel, and SBE Seasave software. Two additional sensors were attached to the CTD frame: A Wetlabs turbidity/chlorophyll sensor and a Wetlabs CDOM sensor. Furthermore, an underwater vision profiler (UVP) was mounted on the CTD frame. A Valeport altimeter system was used during the cruise for bottom distance detection of the CTD. The CTD system performed without problems throughout the whole cruise.

5.5.2 Discrete Seawater Sampling with the CTD Rosette

A diverse suite of discrete water samples was collected during the cruise from vertical CTD/RO casts for later analysis on shore. Chemical and biological parameters associated with organic matter composition and microbial activity were sampled in order to investigate the processes that affect the turnover of organic matter in the deep ocean offshore Northern Chile.

At one CTD/RO station from each of the three working areas water samples were collected for: (i) DOM analysis including dissolved organic carbon (DOC), total dissolved nitrogen (TDN), dissolved organic phosphorous (DOP), dissolved combined carbohydrates (dCCHO) and dissolved amino acids (dAA); (ii) non-sinking organic matter components, such as transparent exopolymeric particles (TEP) and coomassie stainable particles (CSP) following the procedures described in Alldredge et al. (1993) and Long and Azam (1996); (iii) particulate organic matter (POM) analysis including particulate organic carbon and nitrogen (POC/N) content, pigment and lipid compositions, metatranscriptomics, metaproteomics and metagenomics; (iv) analysis of the abundance, distribution and community structure of pico- and nano phytoplankton as well as bacteria and viruses using flow cytometry; (v) microbial process rates including chemoautotrophic production, heterotrophic biomass production and extracellular enzyme activity. Additionally, dissolved inorganic nutrient samples were collected. For each of the three casts, we collected samples for all DOM and POM parameters as well as for flow cytometry and nutrients from twelve depths covering the entire water column. For chemoautotrophic production, fewer samples were collected because of the more time-consuming sample processing, which includes incubations. Similarly, metaproteomic & metagenomic samples were collected from selected depths due to large water requirements for these parameters.

All DOM, POM, non-sinking organic matter and flow cytometry samples were shipped cooled or frozen to GEOMAR for further analysis in the Engel lab at GEOMAR, while microbial process rates were determined on board. To determine chemoautotrophic production, 14C uptake measurements were conducted in the dark. Microbial heterotrophic biomass production was determined using the 3H-leucine incubation method (Kirchman et al. 1985, Smith and Azam 1992). Extracellular enzymatic activity of the bulk microbial community was measured using the fluorogenic substrates. Hydrolysis rates of five different enzymes were measured according to Hoppe (1983) as described in Baltar et al. (2016) and Riemann et al. (2002).

5.5.3 Profiling Optical Observations with an Underwater vision profiler (UVP5)

To study the composition and distribution of marine particles (plankton and marine snow aggregates), an Underwater Vision Profiler UVP5 (Picheral et al. 2010), was mounted to the CTD/RO to take images during every CTD/RO cast. The UVP5 system uses computerized optical technology with custom lighting to acquire digital images in-situ down to a depths of 6000 m. The camera takes greyscale images of plankton particles within a size spectrum from a few µm up to several cm (Fig. 5.26). The UVP5 data (particle abundance in different size classes as well as image data) will be matched to calibrated CTD/RO profiles and stored and sorted into taxonomic categories using Ecotaxa (https://ecotaxa.obs-vlfr.fr/).

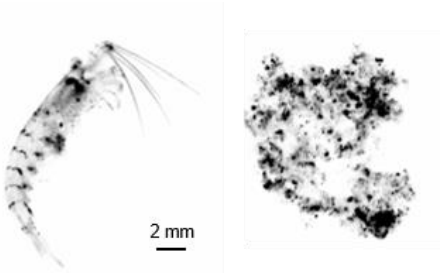

Fig. 5.26 Example of plankton (left) and marine snow (right) images taken with the UVP5 during SO288.

5.5.4 Marine Snow Catcher (MSC)

Marine snow is an abundant and ubiquitous component of the marine water column, which affects the biology and chemistry of the ocean in multiple ways. For example, marine snow aggregates transport part of the photosynthetically fixed carbon into the deep ocean, where it can serve as a source of reactive substances for deep-sea microbial communities. During SO288, we used two Marine Snow Catchers (MSC, OSIL) to collect marine snow aggregates. Due to time constraints, MSCs could only be deployed in working AREA1. Here, one snow catcher was deployed to a depth of 50 m, which was near the base of the photic zone (as seen from the chlorophyll sensor readings of the preceding CTD/RO cast) and the second one to a depth of 1500 m. After deployment, aggregates were left to settle to the base of the MSC on deck for about 3 h. Aggregates were then collected with a serological pipette and preserved for later examination of their structure, chemical composition, and bacterial colonization using light and confocal microscopy.

5.5.5 In-Situ Microbial Incubator (ISMI)

To characterize marine prokaryotic activities at in-situ pressure condition, an in-situ microbial incubator (ISMI) was deployed twice during this cruise to a depth of 1500 m. The first deployment was in working AREA1 and the second deployment in AREA2. The ISMI can collect and incubate seawater at a chosen depth and is also able to fix a certain volume of the incubated samples at specific time intervals. We tested the operation of the in situ incubator and measured ^{3}H-leucine incorporation both at in-situ and at atmospheric pressure conditions (Fig. 5.27).

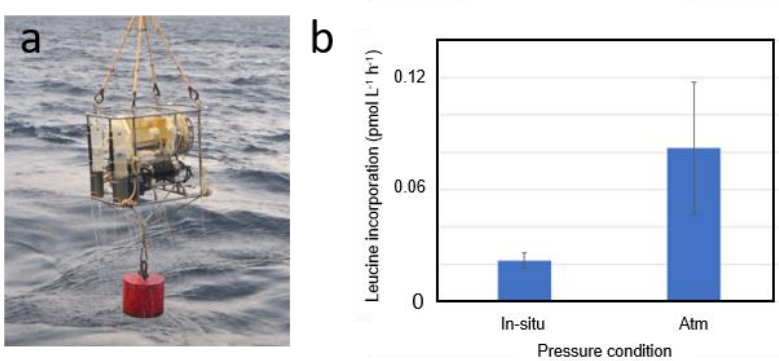

Fig. 5.27 Recovery of the ISMI after the in-situ incubation of 6 hours at a depth of 1500 m. b) Leucine incorporation rates under in-situ and atmospheric pressure conditions (atm).

5.5.6 Onboard Incubation Experiments with Deep-Sea Bacteria

Dissolved organic matter enrichment experiments. Water from the surface (collected with the ship's surface water intake system) and the deep ocean (collected with the CTD/RO) was used for experimental studies on board. From the respective water, dissolved organic macromolecules were concentrated in 0.22 µm pre-filtered seawater by ultrafiltration. The ultrafiltration technique separates compounds according to their molecular weight through a semipermeable membrane. In the enrichment experiments a membrane with a molecular weight cut-off of 1 kDa was used. Solutes of higher molecular weight are retained in the retentate, while lower molecular weight solutes pass through the membrane in the permeate. After enrichment of the organic compounds, viruses were removed from the retentate with a 40 kDa membrane and the concentrate was incubated in deep-ocean water from 1500 m collected with the CTD/RO containing the natural bacterial communities. The samples were incubated at in-situ temperature (2.5 °C) and at 6.5 °C in the climate labs of the ship. Samples for the composition of dissolved organic matter and the activity of microbes (see 5.5.2 for types of analysis) were collected at the start of the experiment and two additional time points (five days and seven days after the start of the experiments). The experiments will run for 365 days and incubation bottles were shipped cooled (4 °C) to GEOMAR for additional sampling on shore. With these long-term experiments, we will investigate the effect of source, lability, composition and concentration of organic matter on microbial processes relevant for the turnover of organic matter in the deep ocean. In particular, we will test whether the dilute concentrations of organic compounds in deep waters hamper the bacterial consumption of molecules that would be reactive when present in higher concentration. The setup of the experiment will also test the impact of the source of organic matter (i.e., surface versus deep ocean) and temperature on the ability of deep-ocean bacteria community to degrade organic matter.

Particulate organic matter enrichment experiments. Particulate organic matter has been identified as major source of reactive substances for deep-sea microbial communities. However, most studies only analyze solid particles and aggregates made in the laboratory from pure cultures, while the role of carbon-rich marine gels reaching the meso- and bathypelagic ocean is rather unknown. With on-board experiments, we will test the potential of gel particles generated from natural dissolved organic matter to stimulate heterotrophic bacterial activity in deep-ocean samples. We artificially generated gel particles by adding alginic acid as binding agent to the enriched dissolved organic matter from the surface waters obtained via ultrafiltration as described above. Gel formation was confirmed via microscopy and then concentrated gels were re-suspended in deep-ocean water to study the response of the deep-sea bacterial communities to the organic matter supply derived from gels. Samples for microbial growth and activities, as well as gel particle concentrations were collected over 7 days. Additionally, samples for visualization and quantification of bacterial cells attached to gel particles using confocal laser scanning microscopy after staining with fluorescent probes were collected.

5.6 Expected Results

(D. Lange[1], H. Kopp[1], Shipboard Scientific Party)

[1]GEOMAR

The primary aim of the GeoSEA survey is to monitor surface deformation in response to the tectonic state of the plate interface. The state of locking of the megathrust at depth may range from freely sliding to creeping to partially or fully locked (Fig. 5.28).

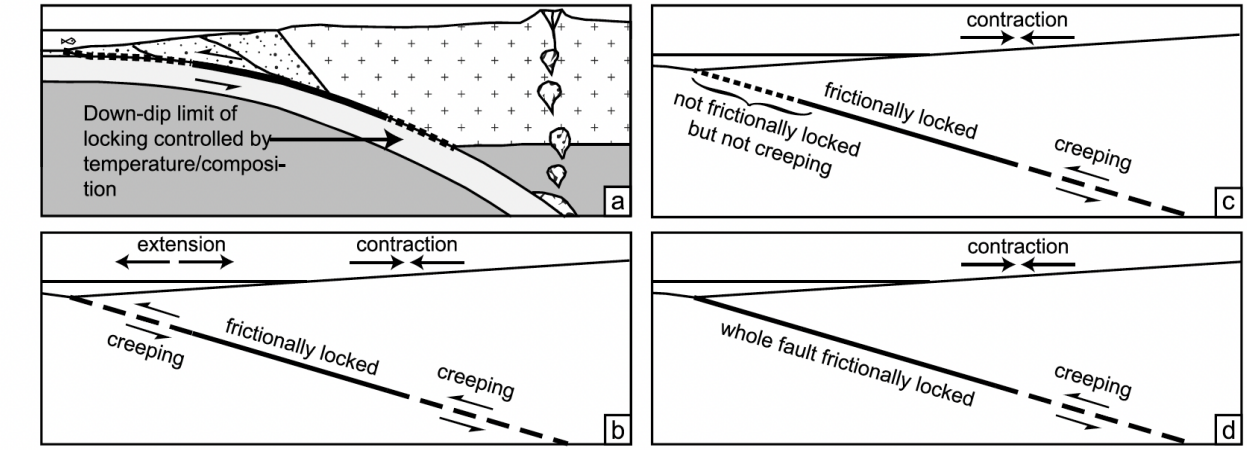

Fig. 5.28 Surface deformation versus plate interface locking at depth. Surface contraction is expected for a fictionally locked megathrust, whereas extension is associated with a creeping interface. From Almeida et al., 2018.

A first evaluation of the GeoSEA geodetic data set indicates that the resolution from our 2.5 years survey will be sufficient to resolve the horizontal strain rate. The final data set comprises 1.261.022 baseline measurements in-between stations located on the seafloor.

Baseline estimation for AREA2 and AREA1 will be conducted over the course of the next months. For AREA2, there are only 1.5 years of high-resolution pressure data. We target to obtain baselines based on the measured sound velocity. Alternatively, we might derive sound speed from the travel time measurement of stations located close by or on one side of the fault.

Baselines estimation of AREA1 suffers from significant drift of the sensors, mapping into the baseline.

In AREA3, where we measure baseline changes with 0.5 mm precision, our in-situ observation of seafloor deformation shows no baseline change. A more in-depth investigation, including directional dependency of deformation, will be the next step. Furthermore, pressure data for all three networks do not show deformation and a very high resolution on short-term water depth changes. The pressure measurements indicate the absence of sudden pressure changes and hence the lack of vertical crustal deformation. Comparing strain estimates for AREA3 with different locking scenarios (Fig. 5.29), we find that the network would have detected movement if this would have the velocity of the downgoing plate (6.6 cm/yr), and locking would start 20 km east of the trench.

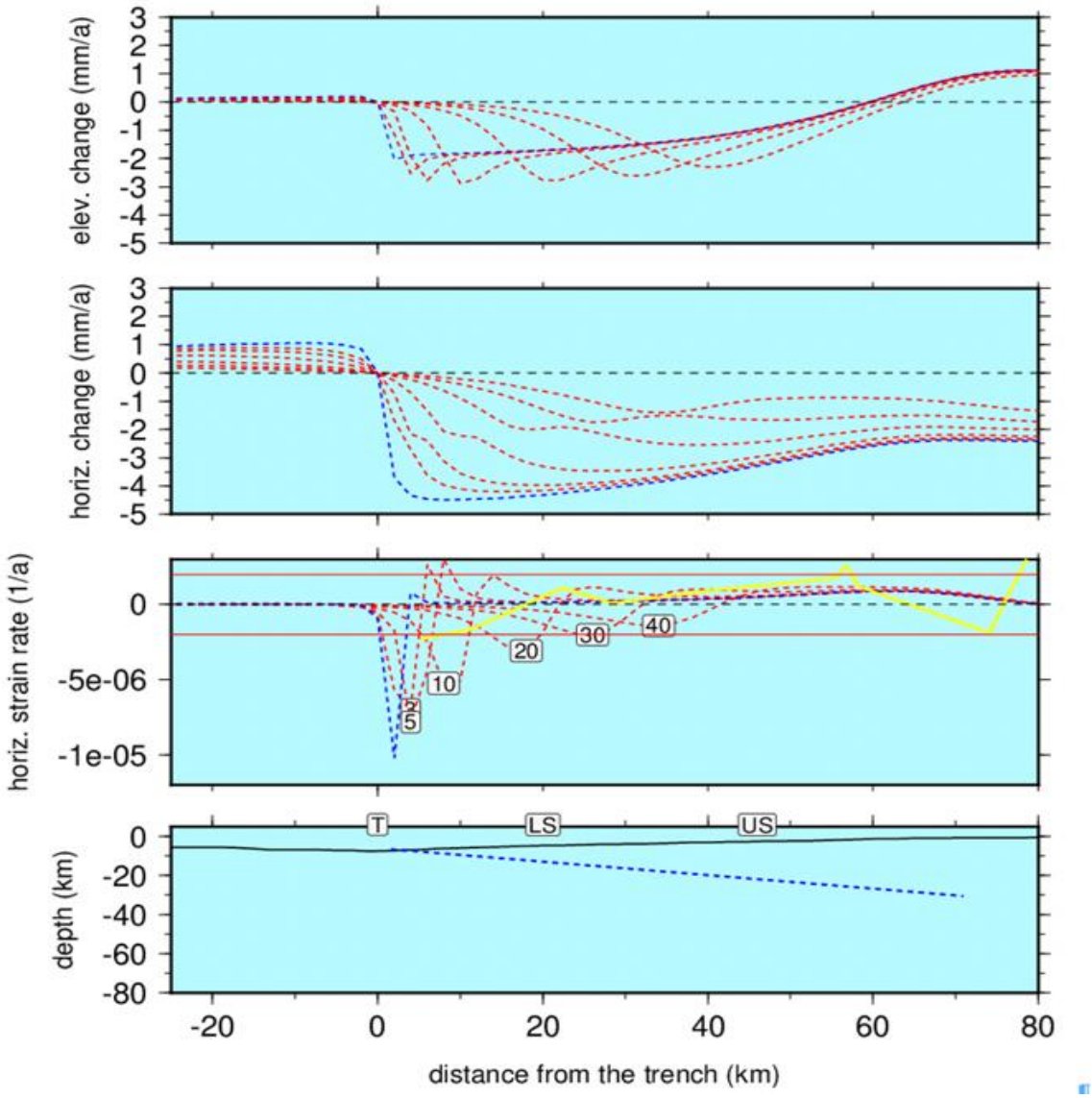

Fig. 5.29 Modelled vertical displacements and strain for different locking scenarios compared with horizontal strain from geodetic land-stations (GPS). The blue dashed line indicates locking from the trench up to 70 km away from the trench. The red dashed lines indicate models with varying locking distances starting 3,5,10,20,30 and 40 km away from the trench. a.) Elevation changes for different locking models with increasing distance from the trench. b.) Horizontal displacements for the different locking models. c.) Horizontal strain rates for the different locking models. Horizontal red lines show the resolution capability of the geodetic network. Yellow line is the postseismic locking extrapolated from GPS land-stations (J. Bedford, pers. comm.). d.) Model geometry with the location of the trench (T) and the lower slope network (LS, AREA3) and the upper slope network (US, AREA1).

6 Station List SO288

6.1 Overall Station Lists

ROV dives during SO288.

Station Number	Dive No.	Date	Time Start	At Bottom	Off Bottom	Time End	Location	Depth	ROV Bottom Time
SO288		**2022[UTC]**	**[UTC]**	**[UTC]**	**[UTC]**	**[UTC]**		**[m]**	**[h]**
Test	310	15.01	Harbour Test Guayaquil., Ecuador						
003ROV01	311	26.01	12:30	14:06	22:22	23:55	GeoSEA AREA 1	2850	08:16
005ROV02	312	27.01	12:35	13:52	19:41	21:09	GeoSEA AREA 1	2850	05:49
008ROV03	313	28.01	12:05	13:20	20:05	21:23	GeoSEA AREA 1	2850	06:45
010ROV04	314	29.01	12:03	13:45	18:49	21:00	GeoSEA AREA 2	4100	05:04
019ROV05	315	01.02	12:00			21:00	GeoSEA AREA 3	5100	--
029ROV06	316	04.02	12:06	14:27	20:24	23:00	GeoSEA AREA 3	5300	05:57
031ROV07	317	05.02	16:34	18:58	23:04	01:49	GeoSEA AREA 3	5400	04:06
033ROV08	318	06.02	14:45	17:09	19:21	21:47	GeoSEA AREA 3	5400	02:12
035ROV09	319	07.02	12:25	14:35	17:29	19:50	GeoSEA AREA 3	5300	02:54
Total: 8 scientific / recovery dives + 1 abandoned dive									**41:03**

GeoSEA recovery coordinates and times.

Station No.	Latitude (°) ROV	Longitude (°) ROV	Depth	Depth	Recov. Date	Recov. Time	S/N
SO288	**[S]**	**[W]**	**ROV [m]**	**Multibeam [m]**	**2022**	**[UTC]**	
Area 1							
A107	-70° 49.883'	-20° 47.919'	2869.5	2867.1	26.01	15:35:13	284790-010
A108	-70° 50.052'	-20° 47.645'	2861.6	2858.3	26.01	18:45:16	284790-001
A106	-70° 49.505'	-20° 47.826'	2844.9	2843.4	26.01	22:17:06	284790-009
A103	-70° 49.059'	-20° 47.606'	2750.1	2741.3	27.01	14:27:28	284790-004
A104	-70° 48.581'	-20° 47.399'	2621.5	2617.7	27.01	19:31:45	284790-005
A105	-70° 49.434'	-20° 48.168'	2871.0	2880.9	28.01	14:11:44	284792-008
A101	-70° 48.942'	-20° 47.964'	2743.0	2731.9	28.01	17:38:21	284790-002
A102	-70° 48.507'	-20° 47.721'	2609.8	2603.3	28.01	20:00:30	284790-003
Area 2							
A201	-71° 43.927'	-21° 3.438'	4130.1	4110.9	29.01	17:26:09	284791-006
A202	-71° 43.997'	-21° 3.154'	4128.8	4104.8	29.01	16:24:05	284971-008
A203	-71° 44.217'	-21° 3.503'	4084.3	4061.4	29.01	18:44:14	284791-009
A204	-71° 44.296'	-21° 3.16'	4059.7	4048.5	29.01	14:53:27	284792-006
A205	-71° 44.226'	-21° 3.402'	4083.5	4060.5	29.01	18:26:37	284791-005
Area 3							
A301	-71° 4.158'	-20° 47.038'	5292.5	5243	04.02	17:27:33	284790-006
A302	-71° 5.045'	-20° 47.571'	5416.9	5367	05.02	19:45:17	284790-007
A303	-71° 3.654'	-20° 46.857'	5243.6	5200	04.02	20:18:04	284790-008
A304	-71° 4.23'	-20° 46.424'	5386.6	5336	06.02	19:19:41	284789-005
A305	-71° 4.659'	-20° 46.838'	5406.6	5357	05.02	23:00:46	284790-010
A306	-71° 4.189'	-20° 46.659'	5342.7	5295	06.02	17:57:33	284789-001

A307	-71° 4.232'	-20° 48.046'	5278.4	5233	07.02	17:21:40	284789
A308	-71° 3.741'	-20° 47.903'	5175.8	5133	07.02	16:07:01	284789-003
A309	-71° 2.779'	-20° 47.694'	5142.5	5098	07.02	14:57:23	284789-004
A310	-71° 3.975'	-20° 47.245'	5269.7	5223	04.02	16:03:20	284791-002

OBS deployment and recovery coordinates and dates.

Station No.	Latitude (°)	Longitude (°)	Deploy. Date	Recov. Date	Depth	Recorder No.
SO288	[°S]	[°W]	2022	2022	[m]	
OBS21	21°03,042	071°425,22	08.02	09.02	4270	011
OBS22	21°03,087	071°43,047	08.02	09.02	4242	005
OBS23	21°03,222	071°43,672	08.02	09.02	4104	007
OBS24	21°03,261	071°44,265	08.02	09.02	4046	017
OBS25	21°03,363	071°44,849	08.02	09.02	4037	013
OBS26	21°03,437	071°45,400	08.02	09.02	4061	014
OBS31	20°47,213	071°06,286	01.02	03.02	5610	011
OBS32	20°49,942	071°06,030	01.02	03.02	5603	005
OBS33	20°46,590	071°05,713	01.02	03.02	5474	007
OBS34	20°46,244	071°05,409	01.02	03.02	5445	017
OBS35	20°45,846	071°05,046	01.02	03.02	5499	013
OBS36	20°45,508	071°04,742	01.02	03.02	5534	014

6.2 Profile Station List

Line no.	Date	Time Start	Time End	Latitude Start	Longitude Start	Latitude End	Longitude End	FFN Start	FFN End
				Start		End			
SO288	2022	[UTC]	[UTC]	xx° xx.x‘	xx° xx.x‘	xx° xx.x‘	xx° xx.x‘		
Survey P2000									
P2001	29.01	23:09:00	01:33:57	21°06,885	071°46,714	21°02,114	071°38,298	180	1041
P2002	30.01	02:06:38	04:11:40	21°00,860	071°39,455	21°04,910	071°46,947	1237	1988
P2003	30.01	04:48:21	06:44:39	21°03,193	071°47,766	20°59,269	071°40,557	2208	2906
P2004	30.01	07:30:06	09:28:00	20°57,513	071°41,664	21°01,171	071°48,439	3179	3883
P2005	30.01	09:47:00	11:50:00	21°02,159	071°48,506	21°05,975	071°41,205	3994	4729
P2006	30.01	12:28:18	14:09:16	21°04,407	071°40,212	21°01,093	071°46,795	4968	5574
P2007	30.01	14:45:57	16:38:58	20°59,331	071°46,079	21°02,516	071°39,432	5794	6472
P2008	30.01	17:28:49	19:13:43	21°04,985	071°40,612	21°01,766	071°47,184	6771	7401
P2009	30.01	19:46:04	21:36:00	21°00,468	071°46,594	21°03,717	071°39,832	7594	8250
P2010	30.01	22:15:00	23:54:00	21°05,457	071°40,651	21°02,383	071°45,775	8475	9085
P2011	31.01	00:32:05	02:31:33	21°03,564	0,71°46,811	21°00,002	071°40,124	9311	10027
P2012	31.01	03:12:01	05:07:50	21°01,695	071°38,923	21°05,815	071°46,315	10270	10965
P2013	31.01	05:39:45	07:52:49	21°04,654	071°47,106	21°00,611	071°39,716	11157	11955
P2014	31.01	08:29:00	10:54:00	21°02,086	071°38,806	21°07,058	071°47,792	12170	13037
Survey P3000									
P3001	01.02	23:05:00	00:44:19	20°50,052	071°05,192	20°45,793	071°01,337	14118	14617
P3002	02.02	01:15:11	02:15:58	20°44,557	071°02,499	20°47,717	071°05,380	14771	15074
P3003	02.02	02:46:10	03:55:46	20°47,004	071°06,889	20°43,780	071°04,114	15225	15574

P3004	02.02	04:41:34	05:36:58	20°45,044	071°02,567	20°47,928	071°05,123	15803	16080
P3005	02.02	06:04:36	07:16:37	20°47,197	071°06,422	20°43,898	071°03,456	16218	16578
P3006	02.02	07:51:03	08:50:00	20°45,041	071°02,225	20°48,016	071°04,841	16750	17041
P3007	02.02	09:17:00	10:26:00	20°47,426	071°06,230	20°44,253	071°03,463	17179	17521
P3008	02.02	11:05:38	12:02:13	20°45,260	071°02,044	20°48,232	071°04,675	17723	18005
P3009	02.02	12:27:34	13:31:30	20°47,643	071°06,004	20°44,432	071°03,193	18133	18452
P3010	02.02	14:10:55	15:11:34	20°45,547	071°01,577	20°48,566	071°04,253	18650	18953
P3011	02.02	16:03:53	17:05:12	20°46,901	071°06,500	20°43,726	071°03,772	19214	19521
P3012	02.02	17:31:22	18:12:35	20°42,976	071°04,990	20°45,189	071°06,609	19652	19858
P3013	02.02	18:27:51	19:25:08	20°45,933	071°05,873	20°48,246	071°02,658	19934	20220
Survey P4000									
P4001	02.02	22:30:00	03:23:19	20°40,436	070°00,220	20°55,512	071°13,708	21065	21654
P4002	03.02	04:40:06	11:49:00	20°55,489	071°13,655	20°33,528	070°54,025	21807	22663
Survey P5000									
P5001	05.02	00:33:00	02:32:00	20°42,342	071°01,529	20°42,520	070°53,115	23124	23835
P5002	05.02	03:02:00	04:26:03	20°44,059	070°53,490	20°43,944	070°59,502	24019	24527
P5003	05.02	04:59:21	07:04:36	20°45,561	070°59,501	20°45,709	070°50,586	24727	25479
P5004	05.02	07:49:57	09:50:08	20°47,875	070°50,676	20°47,549	070°59,249	25751	26472
P5005	05.02	10:31:20	11:25:38	20°49,391	070°59,434	20°49,533	070°55,562	26719	27044
P5006	06.02	03:23:00	05:28:53	20°49,490	070°57,012	20°49,780	070°47,987	27171	27928
P5007	06.02	06:07:17	09:07:59	20°51,691	070°48,029	20°51,390	071°00,904	28159	29243
P5008	06.02	09:47:01	12:30:00	20°53,231	071°00,939	20°53,552	070°49,904	29477	30404
P5009	06.02	23:00:52	02:13:00	20°48,593	071°01,606	20°48,878	070°48,007	30533	31684
P5010	07.02	02:58:00	05:52:36	20°47,807	070°47,807	20°46,512	071°00,273	31851	33003
P5011	07.02	07:57:23	10:37:26	20°43,744	070°56,241	20°54,423	070°56,549	33752	34713
Survey P6000									
P6001	08.02	13:10:00	18:05:11	21°04,737	071°55,354	21°01,645	071°31,963	35075	35667
P6002	08.02	19:05:00	22:49:24	21°01,666	071°32,362	21°04,061	071°50,251	35786	36235
Survey P7000									
P7001	09.02	14:44:00	15:05:00	20°48,192	070°46,951	20°48,164	070°45,501	37379	37538
P7002	09.02	15:41:00	17:19:23	20°46,252	070°45,704	20°46,342	070°52,681	37814	38548
P7003	09.02	17:53:56	19:20:50	20°47,909	070°52,701	20°47,839	070°46,530	38807	39455
P7004	09.02	19:43:11	20:07:12	20°48,886	070°46,131	20°49,783	070°47,552	39589	39807
P7005	09.02	20:25:38	21:05:33	20°49,389	070°48,537	20°46,712	070°48,719	39945	40245
P7006	09.02	21:24:41	21:32:31	20°46,147	070°47,778	20°46,430	070°47,309	40389	40389
P7007	09.02	21:55:00	23:10:57	20°47,509	070°47,582	20°47,574	070°52,963	40617	41186
P7008	09.02	23:25:18	23:32:11	20°47,031	070°53,651	20°46,561	070°53,683	41293	41345
P7009	09.02	23:49:44	00:32:00	20°45,932	070°52,848	20°46,085	070°49,898	41476	41793
P7010	10.02	01:22:00	01:57:00	20°49,038	070°50,186	20°49,115	070°52,710	42163	42427
P7011	10.02	02:40:00	04:04:49	20°47,231	070°52,362	20°47,148	070°46,268	42748	43387
P7012	10.02	04:36:57	06:31:47	20°48,614	070°46,069	20°48,746	070°54,276	43628	44490
P7013	10.02	07:10:25	09:16:18	20°46,902	070°54,298	20°46,732	070°45,333	44778	45721
P7014	10.02	09:46:40	11:47:36	20°48,164	070°45,363	20°48,285	070°53,973	45947	46853
P7015	10.02	12:27:00	13:27:00	20°50,072	070°54,071	20°49,990	070°49,822	47142	47500
P7016	10.02	13:41:00	14:30:00	20°49,427	070°49,153	20°46,087	070°49,308	47695	48071

6.3 Sample Station List

Times and positions of CTD (including UVP5), Marine Snow Catcher (MSC) and In-Situ Microbial Incubator (ISMI) deployments for the biogeochemical and microbiological work during SO288.

Station No.		Date	Gear	Time	Profile/ Sampling depth	Latitude (°)	Longitude (°)	Water depth
SONNE	Working area	2022	[UTC]	[UTC]	[m]	[°S]	[°W]	[m]
SO288_2-2	1	26.01	CTD	01:40	2500	20° 47.887′ S	070° 49.824' W	2870
SO288_2-3	1	26.01	CTD	06:52	1000	20° 47.883′ S	070° 49.827' W	2860
SO288_4-1	1	27.01	CTD	00.10	2500	20° 47.887′ S	070° 49.440' W	2846
SO288_4-2	1	27.01	CTD	02:06	1500	20° 47.843′ S	070° 49.442' W	2846
SO288_4-3	1	27.01	CTD	05:25	1500	20° 47.836′ S	070° 49.444' W	2841
SO288_4-4	1	27.01	CTD	07:22	1500	20° 47.839′ S	070° 49.443' W	2844
SO288_7-1	1	28.01	CTD	01:17	1500	20° 47.651′ S	070° 50.075' W	2862
SO288_7-2	1	28.01	CTD	02:31	1500	20° 47.650′ S	070° 50.059' W	2857
SO288_7-3	1	28.01	CTD	05:41	1500	20° 47.652′ S	070° 50.060' W	2863
SO288_9-1	1	28.01	MSC	22:44	50	20° 47.571′ S	070° 50.104' W	2860
SO288_9-2	1	28.01	MSC	23:17	1500	20° 47.648′ S	070° 50.055' W	2858
SO288_9-3	1	29.01	ISMI	00:40	1500	20° 47.645′ S	070° 50.051' W	2857
SO288_12-1	2	31.01	CTD	12:20	3800	21° 03.609′ S	071° 44.149' W	4060
SO288_12-2	2	31.01	CTD	16:10	3000	21° 03.442′ S	071° 44.130' W	4070
SO288_12-3	2	31.01	CTD	19:32	1500	21° 03.435′ S	071° 44.126' W	4069
SO288_12-4	2	31.01	CTD	21:34	1000	21° 03.442′ S	071° 44.132' W	4074
SO288_28-1	3	03.02	CTD	23:03	1500	20° 46.586′ S	071° 04.617' W	5327
SO288_28-2	3	04.02	CTD	01:19	1500	20° 46.566′ S	071° 04.631' W	5345
SO288_28-3	3	04.02	ISMI	03:03	1500	20° 46.563′ S	071° 04.642' W	5342
SO288_36-1	3	07.02	CTD	20:40	5000	20° 46.565′ S	071° 04.631' W	5340
SO288_36-2	3	08.02	CTD	00:40	1000	20° 46.566′ S	071° 04.633' W	5338
SO288_36-3	3	08.02	CTD	02:33	1000	20° 46.565′ S	071° 04.640' W	5337

7 Data and Sample Storage and Availability

The metadata of the onboard DSHIP-System is collected made publicly available through the Kiel Data Management Team (KDMT), which provides an information and data archival system. This Ocean Science Information System (OSIS-Kiel) is accessible for all project participants and can be used to share and edit field information and to provide scientific data, as they become available. The central system OSIS is providing information on granted ship time with information on the scientific program and the general details down to the availability of data files from already concluded cruises. The transparency on the research activities is regarded as an invitation to external scientists to start communication on collaboration on behalf of the newly available data.

The KDMT will take care as data curators to fulfill the here proposed data publication of the data in a World Data Center (e.g. PANGAEA) which will then provide long-term archival and access to the data. The data publication process will be based on the available files in OSIS and is therefore transparent to all reviewers and scientists. This cooperation with a world data center

will make the data globally searchable, and links to the data owners will provide points of contact to project-external scientists. The seismic, bathymetric and hydro-acoustic raw data and video footage as well as processed seismic data will be archived on a dedicated server at GEOMAR, which is daily backed up and which holds all data since the founding days of GEOMAR. OSIS provides contact information for these large data files.

Availability of metadata in OSIS-Kiel(portal.geomar.de/osis): 2 weeks after the cruise

Availability of data in OSIS-Kiel (portal.geomar.de/osis): 6 months after the cruise

Availability of data in a WDC/PANGAEA (www.pangaea.de): 5 years after the cruise

All hydroacoustic data collected during SO288 are stored in facilities of GEOMAR Helmholtz-

Zentrum für Ozeanforschung Kiel (responsible Prof. Dr. H. Kopp). Multibeam field data are stored at the bathymetric data centre of the Bundesamt für Seeschiffahrt und Hydrografie.

Table 7.1 Overview of data availability

Type	Database	Available	Free Access	Contact
AMT Data	GEOMAR	May 2022	June 2027	dlange@geomar.de
MCS Data	GEOMAR	May 2022	June 2027	hkopp@geomar.de
OBS Data	GEOMAR	May 2022	June 2027	hkopp@geomar.de
ROV Video Footage	GEOMAR	May 2022	June 2027	hkopp@geomar.de
Multibeam	BSH, PANGAEA	May 2022	June 2027	hkopp@geomar.de
PARASOUND	GEOMAR	May 2022	June 2027	hkopp@geomar.de
CTD, ADCP	PANGAEA	May 2022	June 2027	kbecker@geomar.de
Ship's Metadata	BSH, OSIS-Kiel	March 2022	March 2022	

8 Acknowledgements

SO288 is the first cruise of RV SONNE to start from a South American port to the Pacific during the COVID-19 pandemic. The ambitious planning and preparation related to the transportation of infrastructure and the safe travel of the scientific and nautical crews would not have been possible without the excellent shore-based administrative and logistical support of the Leitstelle Deutsche Forschungsschiffe, Briese Research and the Projektträger Jülich. We gratefully acknowledge the help of the Foreign Office in Berlin and the German Embassy in Santiago de Chile. We would also like to thank the Government of Chile for granting opportunity to work within their territorial waters. S.H.O.A. and SUBPESCA in Chile are thanked for the efficient permitting process. In particular, we would like to extend our special thanks to Prof. Sergio Barrientos (National Seismological Center and Universidad de Chile) and Prof. Eduardo Contreras-Reyes (Universidad de Chile) for their continued support. We especially thank Captain Tilo Birnbaum and his crew for managing the complicated logistics of the two scientific groups as well as of the large deployment of equipment and for their skillful execution of the complex scientific program. They contributed exceptionally to the pleasant and professional atmosphere on RV SONNE and their strict discipline in adhering to the safety and hygiene measures after the COVID-19 infections on board were confirmed made a decisive contribution to breaking the chains of infection. Thank you also to the participants of the Round Table for their intensive support from shore. The cruise and scientific work were financed by the Bundesministerium für Bildung und Forschung (BMBF) under grants 03F0658I (GeoSEA),

03G0288NA (COMBO) and 03G0288NB (HOMER) with additional funding and use of large-scale equipment from GEOMAR.

9 References

Almeida, R., Lindsey, E. O., Bradley, K., Hubbard, J., Mallick, R., & Hill, E. M., 2018. Can the updip limit of frictional locking on megathrusts be detected geodetically? Quantifying the effect of stress shadows on near-trench coupling. Geophysical Research Letters, 45, 4754–4763. https://doi.org/10.1029/2018GL077785.

Alldredge, A.L., Passow, U. and Logan, B.E., 1993. The abundance and significance of a class of large, transparent organic particles in the ocean. Deep Sea Research Part I: Oceanographic Research Papers, 40(6), 1131-1140.

Baltar, F., Legrand, C. and Pinhassi, J., 2016. Cell-free extracellular enzymatic activity is linked to seasonal temperature changes: a case study in the Baltic Sea. Biogeosciences, 13(9), 2815-2821.

Béjar-Pizarro, M. et al., 2010. Asperities and barriers on the seismogenic zone in North Chile: state-of-the-art after the 2007 Mw 7.7 Tocopilla earthquake inferred by GPS and InSAR data, Geophys. J. Int., 183, 390-406.

Bialas, J., Flueh, E. R., 1999. Ocean bottom seismometers. Sea Technology, 40, 4, 41-46.

Bürgmann, R., Chadwell, D., 2014. Seafloor Geodesy. Annu. Rev. Earth Planet. Sci. 42, 509–534. https://doi.org/10.1146/annurev-earth-060313-054953.

Chadwell, C.D., Hildebrand, J.A., Spiess, F.N., Morton, J.L., Normark, W.R., Reiss, C.A., 1999. No spreading across the Southern Juan de Fuca Ridge axial cleft during 1994–1996. Geophys. Res. Lett. 26, 2525–2528. https://doi.org/10.1029/1999GL900570.

Dunn, S., Hatchell, P., Beukel, A. van den, Vries, R. de, Frafjord, T., 2016. A long-term seafloor deformation monitoring campaign at Ormen Lange gas field. First Break 34, 55–64.

Flueh, E.R., Bialas, J., 1996. A digital, high data capacity ocean bottom recorder for seismic investigations. Int. Underwater Systems Design, 18, 3, 18-20.

Geersen, J., Ranero, C.R., Klaucke, I., Behrmann, J., Kopp, H., Tréhu, A., Contreras-Reyes, E., Barckhausen, U., Reichert, C., 2018. Active tectonics of the Northern Chilean marine forearc and adjacent oceanic Nazca Plate, Tectonics, 10.1029/2018TC005087.

Hoppe, H.G., 1983. Significance of exoenzymatic activities in the ecology of brackish water: measurements by means of methylumbelliferyl-substrates. Marine ecology progress series, 299-308.

Kirchman, D., K'nees, E. and Hodson, R., 1985. Leucine incorporation and its potential as a measure of protein synthesis by bacteria in natural aquatic systems. Applied and environmental microbiology, 49(3), 599-607.

Kopp, H., Lange, D., Hannemann, K., Krabbenhoeft, A., Petersen, F., Timmermann, A., and Scientific Crew SO244-II, 2015. RV SONNE SO244 Leg II Cruise Report, 86 pp.

Lange, D., Bedford, J.R., Moreno, M., Tilmann, F., Baez, J.C., Bevis, M., Krüger, F., 2014. Comparison of postseismic afterslip models with aftershock seismicity for three subduction-zone earthquakes: Nias 2005, Maule 2010 and Tohoku 2011. Geophys. J. Int. 199, 784–799. https://doi.org/10.1093/gji/ggu292.

Lange, D., Kopp, H., Royer, J-Y., Henry, P., Cakir, Z., Petersen, F., Sakic, P., Ballu, V., Bialas, J., Özeren, S., Ergintav, S., Géli, L., 2019. Interseismic Strain Build-up on the Submarine

North Anatolian Fault Offshore Istanbul, Nat. Comm., 10:3006, doi:10.1038/s41467-019-11016-z.

Lay, T., Yue, H., Brodsky, E.E., An, C.,2014. The 1 April 2014 Iquique, Chile, Mw 8.1 earthquake rupture sequence. Geophys. Res. Lett., 41, 2014GL060238. doi: 10.1002/2014GL060238.

Leroy, C.C., Robinson, S.P., Goldsmith, M.J., 2008. A new equation for the accurate calculation of sound speed in all oceans. J. Acoust. Soc. Am. 124, 2774–2782. https://doi.org/10.1121/1.2988296.

Long, R.A. and Azam, F., 1996. Abundant protein-containing particles in the sea. Aquatic Microbial Ecology, 10(3), 213-221.

Ma, B., Geersen, J., Lange, D., Klaeschen, D., Grevemeyer, I., Contreras-Reyes, E., Petersen, F., Riedel, M., Xia, Y., Tréhu, A., Kopp, H., 2022. Megathrust reflectivity reveals the updip limit of the 2014 Iquique earthquake rupture, Nat. Comm., in review.

McGuire, J.J., Collins, J.A., 2013. Millimeter-level precision in a seafloor geodesy experiment at the Discovery transform fault, East Pacific Rise. Geochem. Geophys. Geosystems 14, 4392–4402. https://doi.org/10.1002/ggge.20225.

Petersen, F., Kopp, H., Lange, D., Hannemann, K., Urlaub, M., 2019. Invited Review Article: Measuring tectonic seafloor deformation and strain-build up with acoustic direct-path ranging, J. Geodyn., 124, 14-24, 10.1016/j.jog.2019.01.002.

Petersen, F., Lange, D., Ma, B., Grevemeyer, I., Geersen, J., Klaeschen, D., Contreras-Reyes, E., Barrientos, S., Tréhu, A., Vera, E., Kopp, H., 2021. Relationship between subduction erosion and the up-dip limit of the 2014 Mw 8.1 Iquique earthquake, Geophysical Research Letters, 48, e2020GL092207. https://doi.org/10.1029/2020GL092207.

Picheral, M., Guidi, L., Stemmann, L., Karl, D.M., Iddaoud, G. and Gorsky, G., 2010. The Underwater Vision Profiler 5: An advanced instrument for high spatial resolution studies of particle size spectra and zooplankton. Limnology and Oceanography: Methods, 8(9), 462-473.

Riemann, L. and Azam, F., 2002. Widespread N-acetyl-D-glucosamine uptake among pelagic marine bacteria and its ecological implications. Applied and environmental microbiology, 68(11), 5554-5562.

Schurr, B., et al., 2014. Gradual unlocking of plate boundary controlled initiation of the 2014 Iquique earthquake. Nature 512, doi: 10.1038/nature13681.

Smith, D.C. and Azam, F., 1992. A simple, economical method for measuring bacterial protein synthesis rates in seawater using 3H-leucine. Mar. Microb. food webs, 6(2), 107-114.

Wang, K., Hu, Y., He, J., 2012. Deformation cycles of subduction earthquakes in a viscoelastic Earth, Nature, 484, 327-332.

Yamamoto, R., Kido, M., Ohta, Y., Takahashi, N., Yamamoto, Y., Pinar, A., Kalafat, D., Özener, H., Kaneda, Y., 2019. Seafloor Geodesy Revealed Partial Creep of the North Anatolian Fault Submerged in the Sea of Marmara. Geophys. Res. Lett. 46. https://doi.org/10.1029/2018GL080984.

10 Abbreviations

AD	Analog-to-digital
AUV	Autonomous Underwater Vehicle

BAT	Battery capacity in %
CSP	Coomassie stainable particles
CTD	Conductivity, Temperature, Pressure (Depth) Sensor
DOM	Dissolved organic matter
GeoSEA	Geodetic Earthquake Observatory on the Seafloor
HRT	High-resolution temperature
INC	Inclination
ISMI	In-Situ Microbiological Incubator
MCS	Multichannel Seismic
MSC	Marine Snow Catcher
OBS	Ocean Bottom Seismometer
OMP	Outbreak Management Plan
POM	Particulate organic matter
POC/N	Particulate organic carbon and nitrogen
PRS	Pressure
ROV	Remotely Operated Vehicle
RU	Remote Unit
SSP	Sound Speed Sensor
TEP	Transparent exopolymeric particles
TPR	Temperature sensor
UTC	Universal Time Coordinated
UVP	Underwater vision profiler

11 Appendices

11.1 Selected Pictures of Shipboard Operations

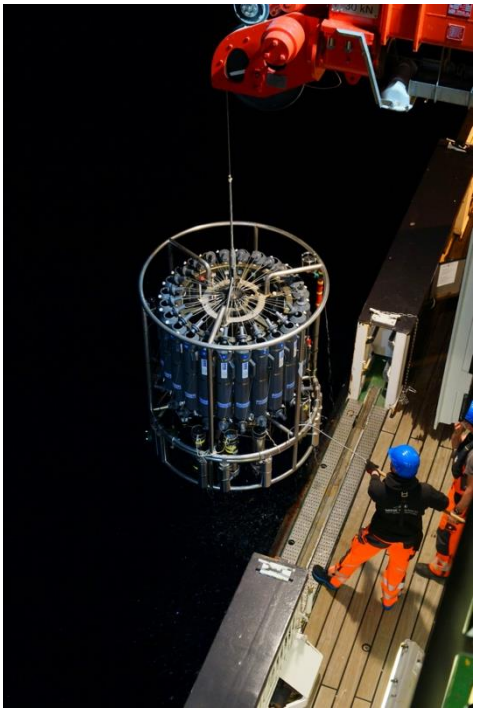

.

Fig. 11.1 CTD cast.

Fig. 11.2 ROV recovery.

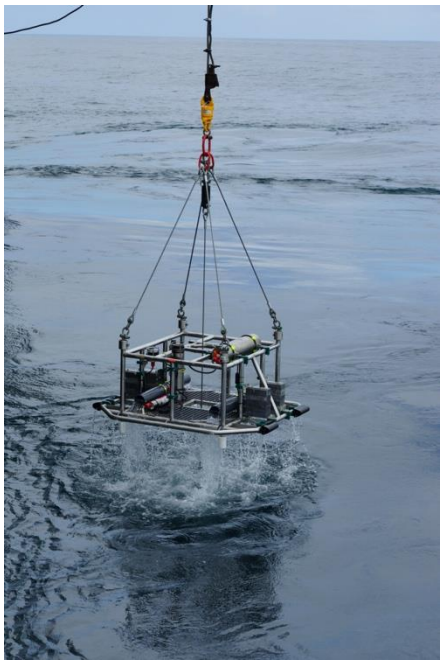

Fig. 11.3 Tripod recovery frame.

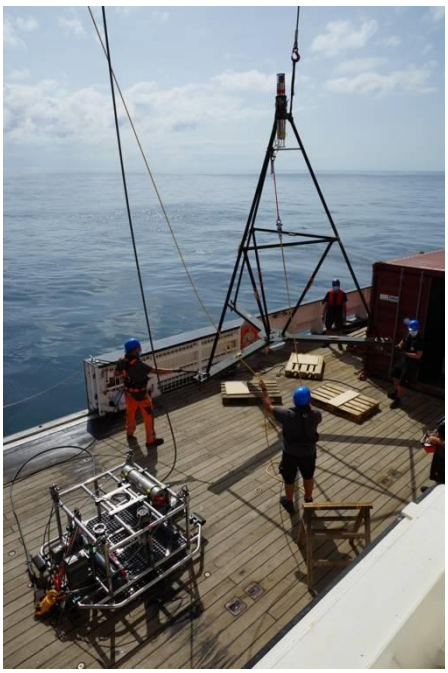

Fig. 11.4 GeoSEA tripod upon recovery.

Fig. 11.5 OBS upon deployment.

Fig. 11.6 G-gun array upon deployment.